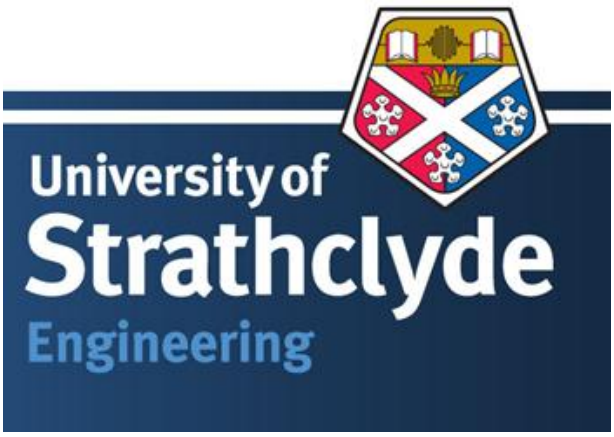

CFD modelling of flow distortion using OpenFOAM

Sylvie Fabre

MPhil

2012

University of Strathclyde

Department of Mechanical and Aerospace Engineering

This thesis is the result of the author's original research. It has been composed by the author and has not been previously submitted for examination which has led to the award of a degree.

Signed:

Date:

Abstract

This thesis presents a computational fluid dynamic (CFD) study of flow related to wind engineering. The open source CFD code OpenFOAM was applied to three cases (i) flow over an oil platform, (ii) flow over a complex terrain and (iii) flow over a met mast. In order to verify the results, experimental work was undertaken using a low speed wind tunnel. In general, the CFD results showed an excellent concurrence with the wind tunnel data. This confirming that correctly used, open source CFD may be applied to wind engineering flows with confidence.

Contents

Acknowledgements

I would like to express my sincere gratitude to my principal supervisor Dr Mathew Stickland for his support, knowledge and patience. Much gratitude should also be expressed to Dr Thomas Scanlon for his encouragements and expertise in CFD modelling. The project would not have taken place without the financial backup of the European project NORSEWInD. I would like to thank Mr and Mrs Andrew and Monica Oldroyd of Oldbaum Services ltd for making this project possible. Finally, I would like to thank Rob Stewart for the construction of the models and Dr Patricia Krus for her much appreciated advices during the writing of the thesis.

1. INTRODUCTION

1.1 Background

In 2007, European leaders agreed to source 20% of their energy need from renewable sources by 2020. Energy such as wind power can play a major role in realising this ambitious target as wind is a free, clean and renewable fuel that will never run out.

Over the last decade, the wind power sector has grown exponentially in Europe with a power capacity installation going from 9600 MW in 1999 to 74 000 MW by the end of 2009 [1].

Of the total energy capacity of EU, 4.2% now comes from wind power which equals to 142 TWh hours of electricity produced by wind power [2].

Further, the European Environmental Agency published in 2009 an assessment on the environmental and economic constraints of Europe's onshore and offshore wind energy potential [2].

After taking into account environmental and social constraints and production costs, the offshore wind energy potential is estimated around 2600 TWh, whereas onshore wind potential should be of the order of 9600 TWh.

This represents a huge potential considering the 3400 TWh electricity consumption in the EU in 2008 [3].

Onshore wind energy potential is concentrated in the agricultural and industrial areas of north-western Europe, while offshore potential can mainly be found in the low depth areas of the North Sea, Baltic Sea and Atlantic Ocean.

The result of this study can be used as a benchmark for the evaluation of the potential role of the wind energy in Europe, however, this report acknowledges that more detailed data is needed on meteorology, land cover, sea depth and wind turbine technology.

1.2 NORSEWInD

In 2008, the European project FP7 or NORSEWInD project was established to address one of the main challenges ahead for the offshore wind industry which is the availability of good quality wind speed data to facilitate better project planning, accurate yield prediction and a fundamentally better understanding of the offshore working environment. This four year project will create one of the world's biggest dedicated instrumentation networks to acquire wind speed data offshore for the North, Irish, and Baltic Seas and part of the Atlantic coast.

NORSEWInD is made up of 15 organisations and coordinated by Oldbaum Services [4].
It has a clear set of objectives, described in the NORSEWInD webpage [5]:
-Acquisition of real physical data offshore in the Baltic, Irish, North and Atlantic Seas
-Development of a database and associated wind atlas derived from the real data
-Validation of techniques to provide cost effective data anywhere offshore
-Promotion and acceptance of remote sensing in the wind industry
-Development of an advanced short term forecasting system taking advantage of near real time spatio-temporal measurement data.

The acquisition of real physical data offshore in order to assess the local wind condition in the Baltic, Irish, North or Atlantic seas, is one of the first steps to be achieved by the NORSEWInD project. Remote sensing technologies such as LiDAR (Light Detecting and Ranging) were chosen to collect the data as they can gather wind speed measurements at a different heights. These instruments have been installed on top of oil platforms or islands in a variety of locations and velocity measurements of the wind will be collected over a period of months to years. As the hub-height of a wind-turbine should be located between 40 m to 160 m from sea level, measurements will be acquired in this height range whenever possible.
Figure 1 shows a typical set of measurement heights above a platform which will be collected by two types of LiDAR: ZephIR [6] and Windcube [7]. The ZephIR

measures wind speed from a minimum height of 40 m from the deck level or ground. The measurements with the Windcube device start at 60 m height as the accuracy of the measurements at 40 m height with this instrument is questionable [6].

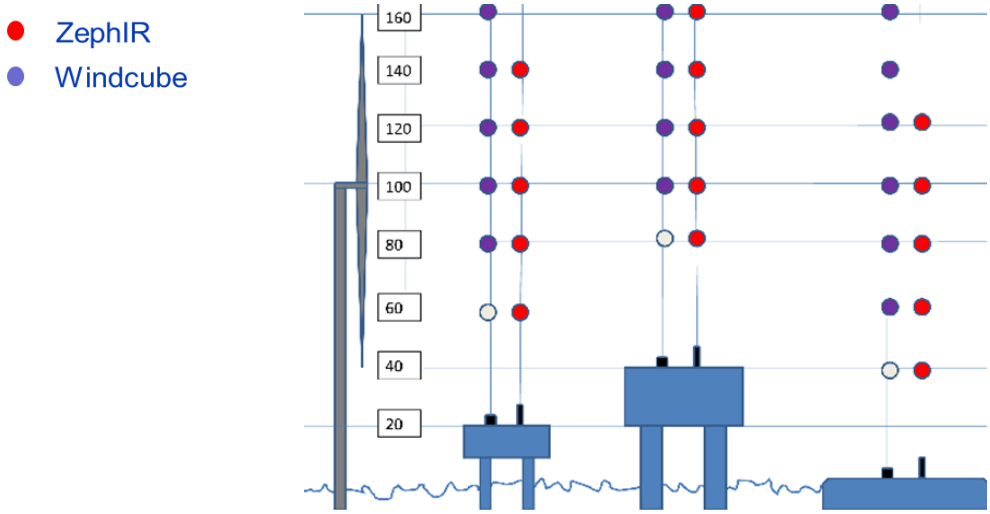

Figure 1: LiDAR measurement heights

1.3 Strathclyde University Task

Due to the fact that offshore installations are large structures, a blockage interference effect of the installations on the wind is expected.

The University of Strathclyde was tasked by NORSEWInD to quantify the blockage effect on the airflow around the platform using Computational Fluid Dynamics (CFD). The computational models will define the area in which the airflow is distorted by the installations. If the LiDAR collects wind speed data outside this area, the raw data will be used as collected. However, if the velocity measurements are within the distortion area, a correction factor, determined by the computational model, will be applied to the raw data to remove the effect of the rig structure. To support the verification of the CFD modelling, a number of sub scale models were created and the flow field surrounding these models was determined experimentally using Strathclyde University's wind tunnel.

1.4 Literature research

1.4.1 Numerical approaches for wind analysis: Historical Perspective and Literature Review

Several numerical simulation techniques currently exist for wind flow analysis, ranging in levels of complexity from simple linear solvers to direct numerical simulation. The principal analysis techniques are described below:

a) **Linear models:** These solve a set of linearized flow equations which contain simplified turbulence and roughness models. The models attempt to correct existing long-term physical data to account for several different effects including object blockage, terrain classification, and land topology.

b) **RANS: (Reynolds Averaged Navier-Stokes):** This CFD technique involves the solution of the time-averaged Navier-Stokes equations with the relevant scales of turbulence being modelled. It is the most well-known and widely-adopted method for practical engineering applications.

c) **Large Eddy Simulation (LES):** Another CFD approach in which the larger scales of turbulence, which contain most of the energy, are directly resolved while the smaller scales, below a certain filter level, are modelled.

d) **Detached Eddy Simulations (DES):** Is a mixture RANS and LES, where RANS model is employed in user-specified regions and LES in others. This hybrid modelling technique affords the user greater flexibility in the computational approach.

e) **Direct Numerical simulations (DNS):** This involves the direct numerical solution of the instantaneous equations that govern fluid flow (the unsteady Navier-Stokes-Fourier equations) using the appropriate length and time scales.

Over recent years the dominant computational method for modelling wind flow has been the linear model or wind atlas technique [8]. In simple terms, this method uses linearized flow equations to correct existing long-term measurements for various different effects including sheltering objects, terrain classification, and domain contours. The advantage of this method is that it is well established and relatively straightforward to apply. The most widely used application of the technique is the WAsP computer code developed by the RISØ National Laboratory in Denmark. WAsP has enjoyed such widespread adoption because the use of linearized flow equations make it able to predict the wind resource with sufficient accuracy and efficiency when the terrain is smooth enough to ensure that the flow remains attached. However, WAsP does have limitations and generates poor predictions when flow separation and recirculation are evident [9]. In an attempt to address this issue, a site ruggedness index (RIX) was proposed as a crude measure of the terrain complexity and hence the extent of flow separation [10]. The RIX is defined as "the fractional extent of the surrounding terrain which is steeper than a certain critical slope". However, despite corrections using the RIX, many researchers concluded that it is not generally advisable to apply WAsP in complex terrain [10-13]. These conclusions, combined with the observation that the increase in wind power production led to sites being selected with increasingly complex terrain [11], meant that alternative computational methods need to be established.

The choice of computational model requires the user to strike a delicate balance between required accuracy and the computational resources available. The range of length and timescales involved in DNS means that significant computational resources are required and the technique is currently impractical for real-world engineering problems. Employed correctly, LES-based modelling is likely to predict results with a higher degree of accuracy compared with RANS models, however, for the large, 3D, complex geometry problems normally encountered in the wind industry, the computational resources for a LES-based solution are currently beyond the reach of the general wind-energy community. Therefore, the current basis for the modelling and simulation of environmental flows in complex terrain is dominated by

the use of linear and RANS-type models. The RANS-type approach was adopted in this thesis.

Given the limitations in the range of topologies that linearized models can handle, CFD is the evident choice as an alternative to WAsP and other linearized approaches, with the RANS approach the most likely choice given the computational restrictions. However, despite the impact of CFD techniques in many areas, such as automotive or aeronautical engineering, it has not yet become common in wind energy engineering [11]. Challenges remain in the numerical modelling of turbulence for atmospheric flows, particularly in complex terrain, and in CFD representations of atmospheric boundary layers [14, 15].

1.4.2 Experimental approaches for wind analysis: Historical Perspective and Literature Review

In the scientific literature, no work for wind flow over oil rigs or through met masts, either experimentally or numerically, appears to exist. This suggests that the work contained in this thesis represents a novel contribution to address the knowledge gap in this field.

Experimental work in this area has focussed principally on flows over representative buildings or urban canopies. In a general review paper, Kanda [16] described progress made in the scale modelling of urban climate. Over 40 relevant studies were cited related to mainly indoor and outdoor experiments that use an array of urban-like flow obstacles or roughness elements such as cubes, blocks, and cylinders. Ahmad *et al* [17] provided a comprehensive literature review on wind tunnel simulation studies in urban street canyons/intersections including, among other parameters, the effects of building configurations, canyon geometries and variable approaching wind directions on flow fields. A review by Tieleman [18] detailed new considerations for the assessment of wind loads on low-rise structures from wind tunnel simulation experiments. Attention was focussed on the aerodynamics of surface-mounted prisms, followed by a discussion of the atmospheric flow characteristics near the surface under a variety of atmospheric and upwind terrain conditions.

In the paper by Cermak [19], a review was presented on wind tunnels capable of simulating natural winds, the boundary-layer wind tunnel (BLWT) and trends in their extensive use in civil engineering practice. BLWTs and data-acquisition systems, as they evolved to meet needs in civil engineering, were described. Advancements were highlighted for the types of wind-load information now available to structural engineers and architects by BLWT tests using advanced data-acquisition systems.

Khanduri *et al* [20] presented an evaluation of wind loads on buildings, carried out mainly by using codes and standards, whose specifications are generally based on wind tunnel tests performed on isolated structures in an open terrain. The paper considered how neighbouring structures may either decrease or increase the flow-induced forces on a building, depending principally on the geometry and arrangement of these structures, their orientation with respect to the direction of flow and upstream terrain conditions.

Stathopoulos [21] presented a review of the current state of the art in computational wind engineering, particularly as it relates to applications of numerical flow modelling for the evaluation of wind effects on buildings and their environment. The variability of computational results was presented and compared with that of wind tunnel measurements. Concerns were expressed regarding the application of the numerical approach in the design practice in cases for which the computational results may not be adequate. Future challenges regarding the improvement of computational wind engineering methodologies were discussed and the importance of identifying resolution and numerical errors was emphasized. Finally, Kasperski [22] showed results from extensive wind tunnel tests on low-rise buildings with flat roofs and introduced a novel alternative wind load distribution with a positive roof pressure.

1.5 Objectives and scope of the thesis

The main purpose of the present work is to validate the open source CFD modelling software OpenFOAM by comparing the experimental data of flow velocities above each model with the CFD simulation.

The first part of this report describes the experimental flow field measurement around a sub-scale model in a wind tunnel. A description of the models and equipment used for the velocity measurements are reported in this section. The principles behind the measurements are explained and the experimental data presented.

In a second part, the open-source CFD software OpenFOAM models are described and the simulation data obtained with this software are reported.

The experimental data and the CFD data are then compared in the third part of the thesis.

2. EXPERIMENTAL FLOW FIELD MEASUREMENT AROUND SUB-SCALE MODELS

2.1 Objectives

Sub-scale model of oil platforms and an island topology, on which the measuring equipment has been placed to collect experimental data offshore, were constructed. The flow distortion was assessed by mounting the model in a wind tunnel and measuring the velocity magnitudes immediately above the model.

2.2 Physical models

Sub-scale models with three very different geometries were part of the study:
-The Beatrice oil platform
-Berlengas island off the Portuguese coast
-The meteorological mast Fino3

2.2.1 The Beatrice Platform

Beatrice is an oil production platform located in the Moray Firth area 24 km from the shore.

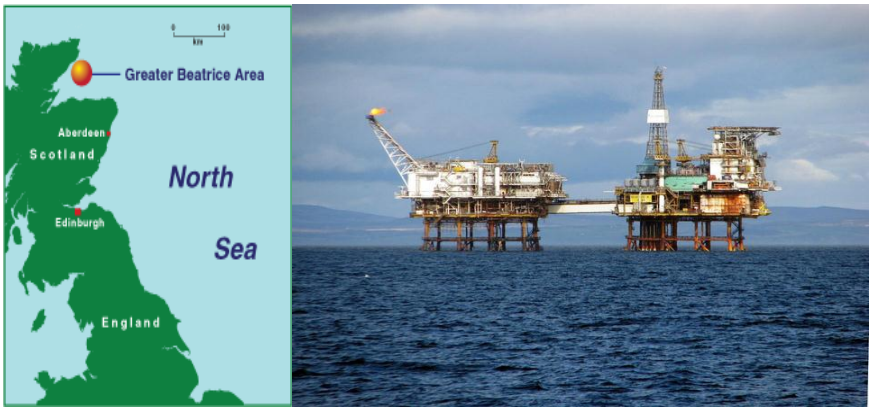

Figure 2: Location and view of Beatrice platform

Beatrice consists of 2 platforms: a drilling rig and a production platform, linked by a bridge. A LiDAR has been installed on one corner of the production platform.
The model, made of plastic, was built at Strathclyde University at the scale 1/160. Figure 3 shows the model in the wind tunnel with some basic dimensions.

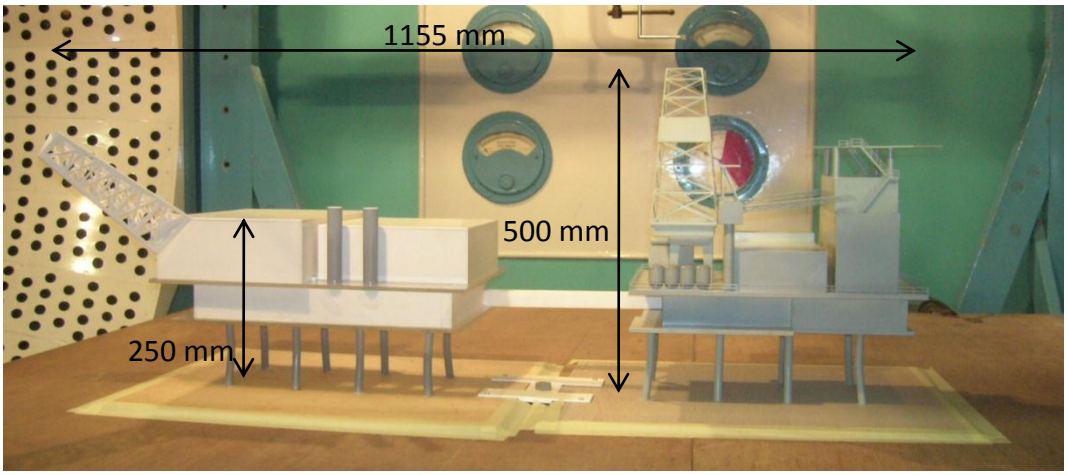

Figure 3: Wind tunnel Beatrice model

2.2.2 Berlengas Island

Berlengas is an island off the west coast of Portugal (Figure 4).
The island is approximately 97 m at its highest point, 1500 m long and 820 m wide. A LiDAR has been located adjacent to the lighthouse near the centre of the island.

Figure 4: View of Berlengas island

A model was created at the scale 1/1250 with a slightly uneven surface texture to initiate roughness effect. The model measured roughly 1200 mm long, 660 mm wide and 80 mm high. A picture of the model in the wind tunnel is reported in Figure 5.

Figure 5: Model of Berlengas in the wind tunnel

2.2.3 Fino3 mast

Fino3 is an offshore meteorological mast mounted on a raised platform. It is located off the west coast of Denmark and measures around 100 m height. A model of part of this mast was created at the scale 1/20 as shown in figure 6 and 7. The dimensions of the wind tunnel model were 90 cm height with a boom of 27 cm long.

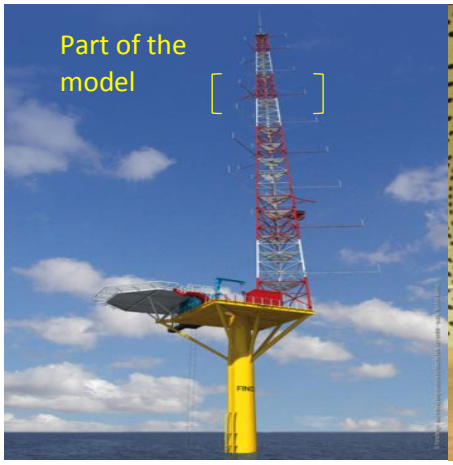

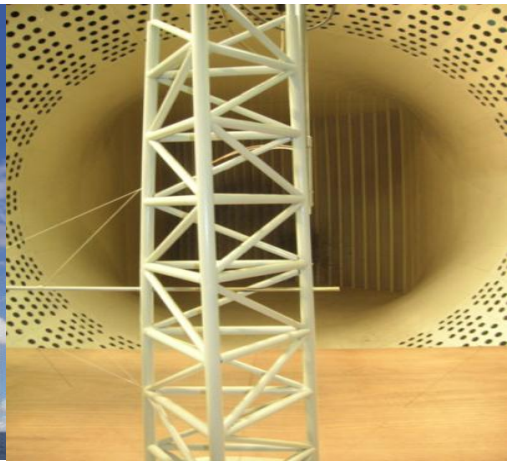

Figure 6: View of actual Fino3 mast ***Figure 7***: Fino3 wind tunnel model

CFD studies were carried out on this model to assess the effect of flow distortion caused by the structure of the mast on the measurements made by the boom mounted instrumentation.

2.3 The equipment

2.3.1 The wind tunnel

The experiments were performed in the Department of Mechanical and Aerospace Engineering's wind tunnel of Strathclyde University. This is a closed circuit wind tunnel with an open working section of 2.5 m length and a nozzle of 1.5 m diameter. An air flow was created by a fan which went through closely spaced turning vanes in order to prevent the flow separating at the sharp corners. The speed flow could vary up to 40 m/s. The circular cross section of the wind tunnel kept blockage effect to a minimum and the turbulence intensity was below 1%.

The model was attached to a working surface positioned 1 m above the ground in the middle of the working section. The working surface was a 1 cm thick board made of wood. Figure 8 represents the Beatrice model in the wind tunnel during a run.

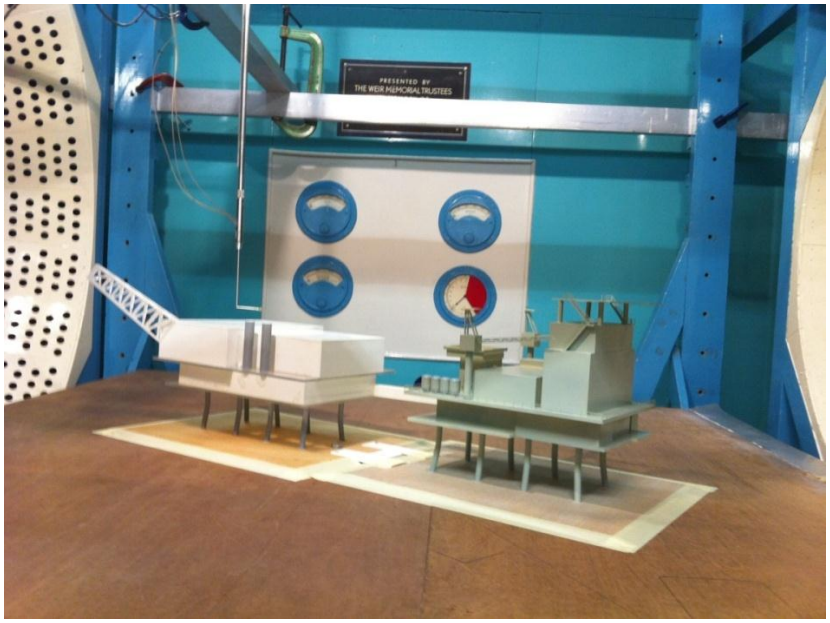

Figure 8: Model set up in the wind tunnel

2.3.2 3D hot wire anemometer

The measuring technique chosen for this study was hot wire anemometry. This technique allowed point measurements of velocity to be taken in a turbulent flow by measuring the three velocity components u, v, w.

Hot wire anemometry is one of the basic measuring techniques used by research scientists and engineers working in fluid mechanics. It is applicable to a wide variety of flows. The working principle is based on the cooling effect of a flow on a heated body and different modes of operation permit measurements of velocity, temperature and concentration.

A computer controlled anemometer with calibrator from DANTEC Dynamics was used to carry out the measurement of velocity around each model.

The measuring equipment, also called CTA anemometer (constant temperature anemometer), consisted of a probe, a Wheatstone bridge with an amplifier, signal conditioner, a converter and a computer as described in Figure 9.

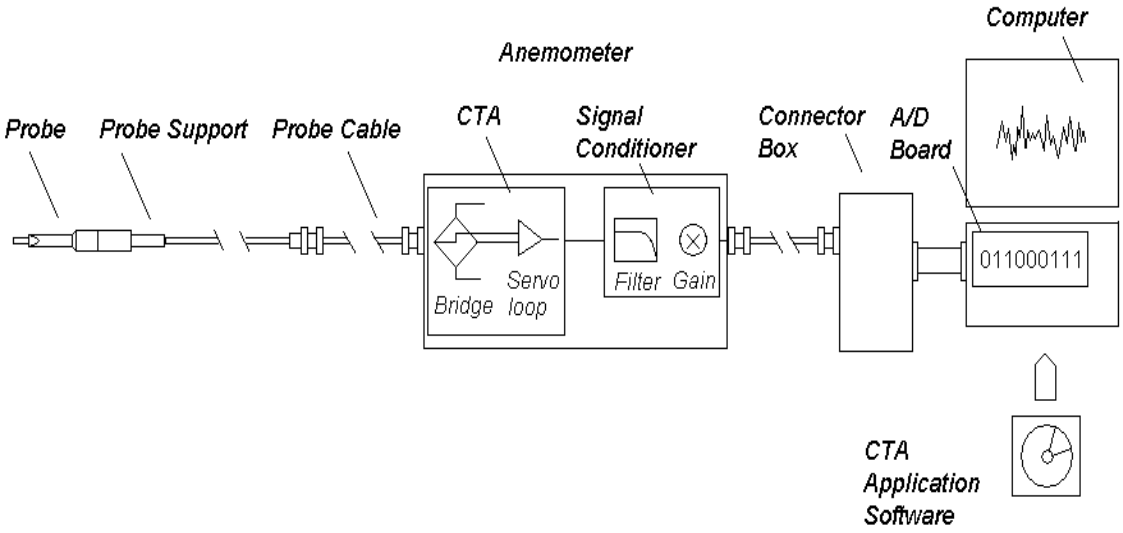

Figure 9: CTA anemometer set up

3 types of probes were used for the experimental study:

i) A single sensor probe 55P11with a 5μm diameter, 1.25 mm long platinum-plated tungsten wire sensor. This probe is recommended for most measurements in one-dimensional flows of low turbulence intensity and was used to measure the mean velocity of the flow delivered by the wind tunnel.

Figure 10: 55P11 probe

ii) A tri-axial sensor probe 55P91 consisting of 5 μm diameter, 3 mm long platinum-plated tungsten wire sensors. This probe is designed for measurements in high turbulence flows of 3 dimensions and it was used for the measurements of the u, v and w velocity components of the flow around the model in the wind tunnel.

Figure 11: 55P91 probe

iii) An omnidirectional probe 55R49 made of quartz, with the sensor deposited as a nickel thin-film protected by a 0.5μm quartz layer. The probe is designed for low velocity measurements in flow fields with unknown flow directions and was used to assess the distortion flow around the Fino3 mast model.

Figure 12: 55R49 Omnidimentional probe

2.4 Experimental procedure

2.4.1 Probe calibration

The probes described above were connected to a Wheatstone bridge and were electrically heated up to a temperature above ambient temperature. The air flowing past the wire or film had a cooling effect.

A servo amplifier kept the bridge in balance by controlling the current of the sensor so that resistance - and hence the temperature of the wire or film - was kept constant. Therefore, the bridge voltage E represents the heat transfer and is thus a direct measure of the velocity.

The 3 probes P91, P11 and R49 were calibrated prior any experiments using an automatic calibration system in order to establish a relation between the CTA output E (V) and the flow velocity U (m/s) (Figure 13).

This was carried out by exposing the probe to a free air jet at known velocities U between 0 m/s and 20 m/ before voltage E was recorded.

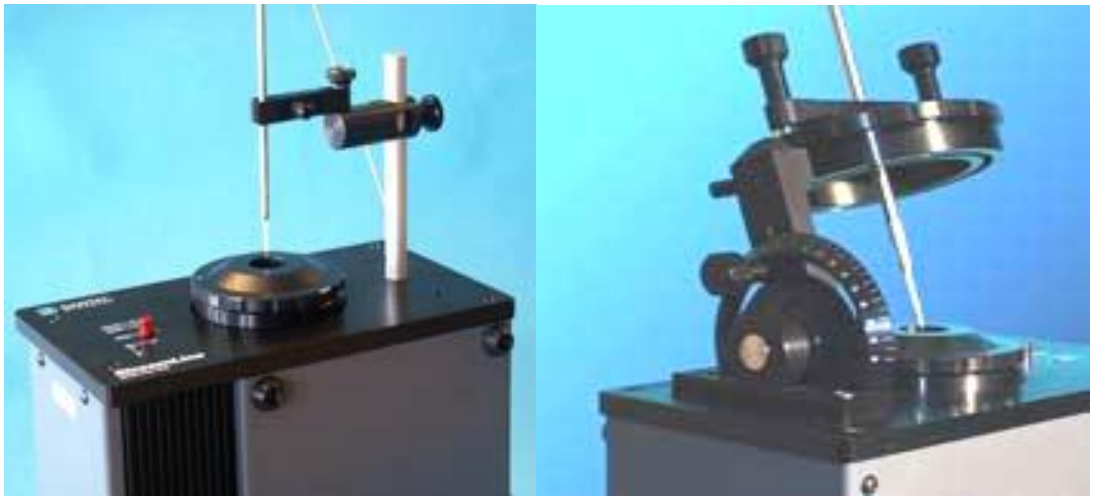

Fig 13: Velocity calibration Directional calibration

A curve fit through the points (E vs U) represents the transfer function to be used when converting data records from voltage to velocity as shown in Figure 14.
For probe P91, having three wires measuring the three components u, v and w, three curves were used to convert voltages to velocity for each components. These three components were then used to calculated the U magnitude.

U	E	T	Pbar	Ecorr
m/s	volts	C	Pa	volts
2.019	1.614	26.0	100.652	1.615
2.622	1.661	26.0	100.654	1.662
3.358	1.705	26.0	100.66	1.706
4.360	1.758	25.9	100.663	1.759
5.621	1.813	25.9	100.66	1.814
7.324	1.876	25.9	100.654	1.877
9.379	1.939	25.9	100.652	1.94
12.121	2.01	25.9	100.652	2.011
15.364	2.08	25.9	100.657	2.081
20.101	2.166	25.9	100.657	2.167

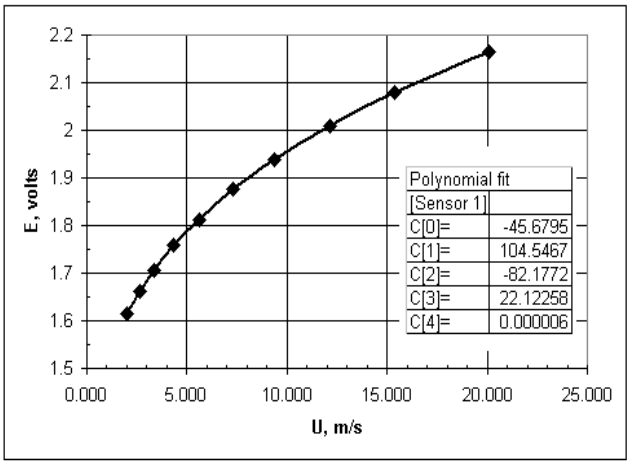

Figure 14: Example of data table and calibration curve

The tri-axial probe P91 was also calibrated for directional sensitivity. To assess this sensitivity, the probe was exposed to an air flow at a specific velocity (10 m/s) while the calibrator inclined the probe by 30 degrees and rotated it every 15 degrees through 360 degrees. The calibration curves are shown in Figure 15.

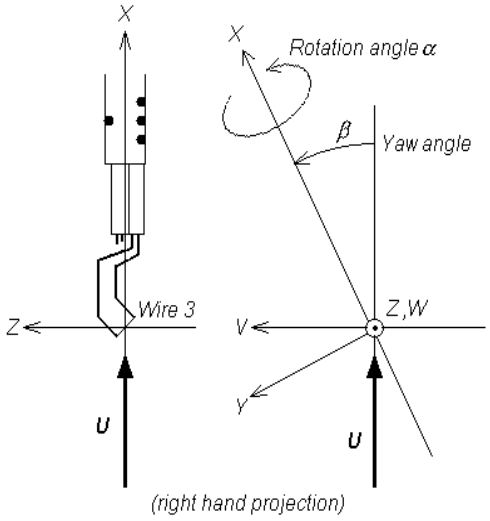

Alfa	E1	E2	E3
deg.	volts	volts	volts
0	1.983	1.841	1.963
15	1.98	1.807	1.981
30	1.975	1.789	1.995
45	1.965	1.798	2.002
300	1.963	1.965	1.922
315	1.985	1.944	1.865
330	1.986	1.916	1.905
345	1.986	1.882	1.938

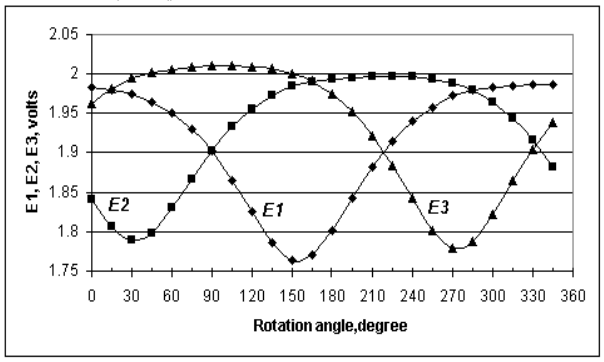

Figure 15: Directional calibration curve

2.4.2 Velocity measurements

The 3D hot wire probe was attached to a traverse allowing the probe to move up and down. Voltage readings were taken on a vertical line above the model with a sampling rate of 10 000Hz.

A single hot wire probe P11 was also positioned upstream in the flow field undisturbed by the presence of the model. This probe took voltage readings at the same time and frequency as the 3D hot wire probe. The P11 readings were used to normalise all velocities measured around the model.

The upstream wind speed was maintained in the range of 15 and 16 m/s during runs.

To simulate the wind approaching the model from different angles the model was rotated relative to the free stream as detailed in Figure 16.

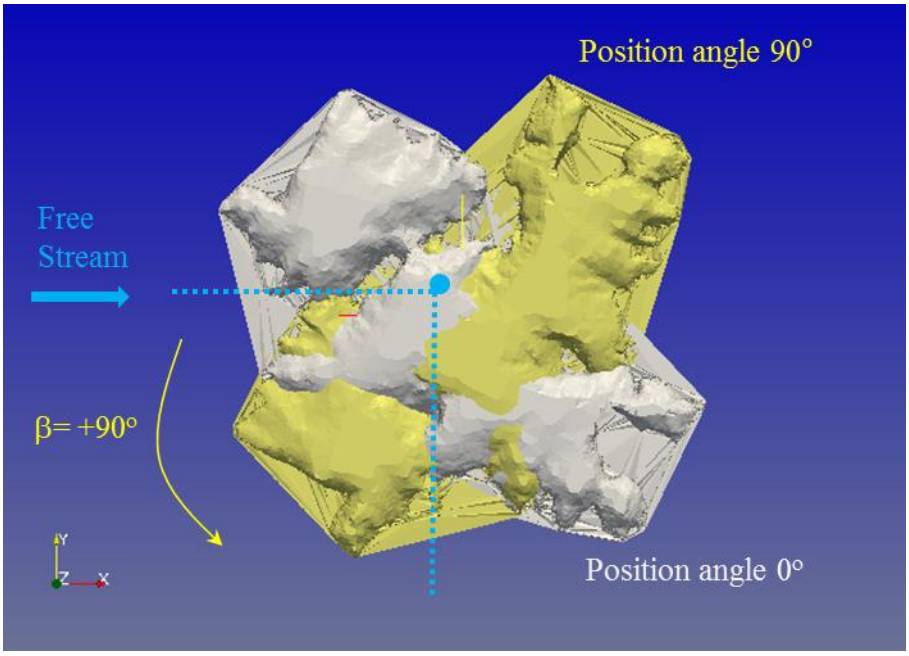

Figure 16: Model rotation to simulate wind direction- Berlengas Island example

When the omnidirectional probe was used to measure the flow around the Fino3 Mast model, the probe was attached directly to the model and thus rotated with the model.

2.5 Experimental data

2.5.1 Velocity profile around the Beatrice platform

The origin of the Beatrice platform coordinate system (x,y,z) was taken as one of the corner of the production platform as highlighted in Figure 17. This position corresponds to the position of the LiDAR taking wind speed measurements for the Norsewind project. Velocity measurements were taken in the wind tunnel by a 3D hot wire probe traversed in the vertical (positive z) direction at this specific position, in increments between 0.6 cm and to 2 cm up to 40.1 cm. In this coordinate system, the x-axis and u-component of the velocity vector were always parallel to the

undisturbed free stream direction. To alter the angle at which the free stream approaches the platform, the model was rotated every 30 degrees around the origin of the coordinate system in an anticlockwise direction when viewed from the above.

Angle 0 would correspond to the free stream aligned with true North. Figure 18 shows the model in the wind tunnel in a position recorded as angle 150°.

The reference height used to normalise the hot wire measurements locations was taken as the production platform height of the wind tunnel model which is 25 cm.

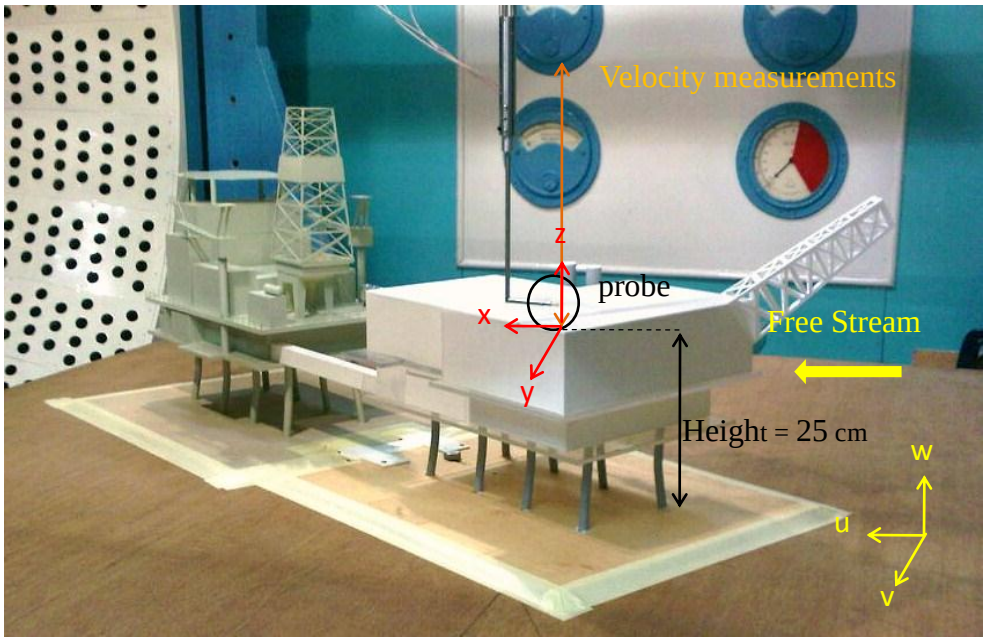

Figure 17: Beatrice platform model in the wind tunnel

Prior to measuring velocity above the model, the undisturbed flow field in the wind tunnel was measured at the traverse position.

Figure 18 represents the ratio between U-magnitude at the traverse location with no model in the wind tunnel and U-magnitude measured upstream by the probe P11. With a ratio varying from 0.982 to 0.992, this graph shows that the reference probe P11 readings can be up to 1.8% higher than the P91 readings.

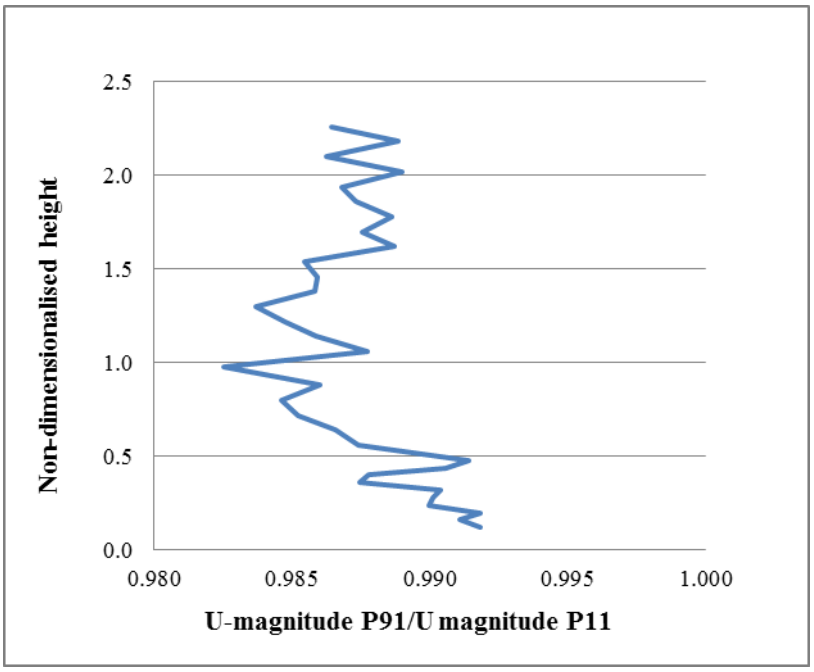

Figure 18: Measurements of the undisturbed flow: ratio U mag P91/U mag P11

This measured difference between the 2 probes had to be taken into account by creating a correction factor CF.

If U_{point} is the U magnitude measured by probe P91 at the location traverse and $U_{reference}$ is the U magnitude measured by the reference probe P11, the correction factor CF is as shown in equation 1.

$$CF = \left[\frac{U_{point}}{U_{reference}}\right]_{empty\ tunnel} \qquad \text{equation 1}$$

To non-dimensionalise the wind speed measured at a specific height with the model in the wind tunnel, the following equation 2 was used:

$$U_{non\ dim} = \frac{U_{point}}{CF * U_{reference}} \qquad \text{equation 2}$$

CF was calculated on each occasion prior to starting a series of experiments.

Velocity profiles were recorded with the model positioned in the wind tunnel at 12 different positions. Four positions are represented in the Figure below.

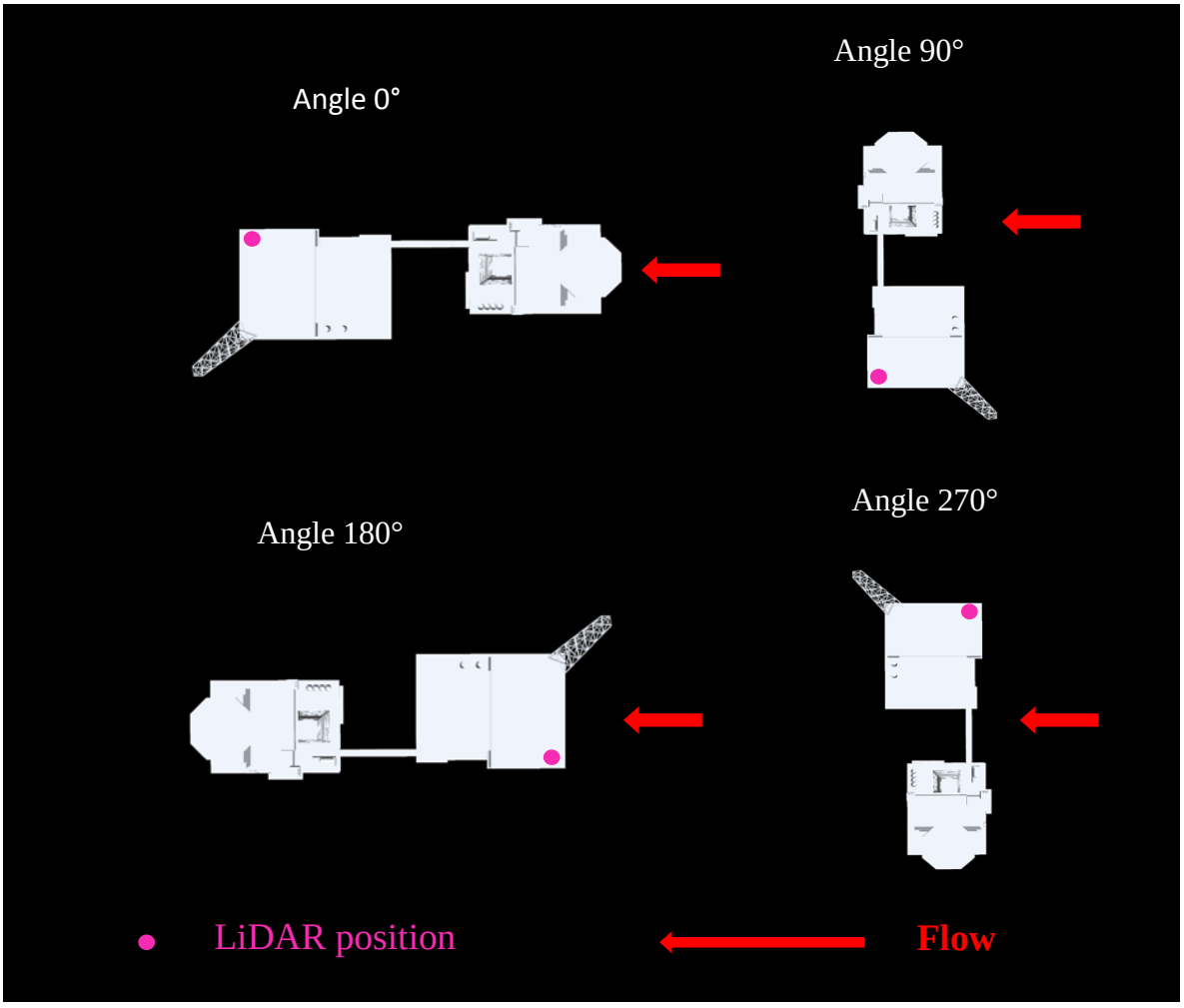

Figure 19: Position of the Beatrice model vs the flow stream

Figure 20 shows the profile for angle 330°. The non-dimensionalised U-magnitude is shown on the x-axis whereas the non-dimensionalised height is placed on the y-axis. Several traverses were undertaken at different times with the model in the same position.

Experiment 1 and 2 were carried out 2 days apart and the difference between the two shows repeatability within approximately 0.5%.

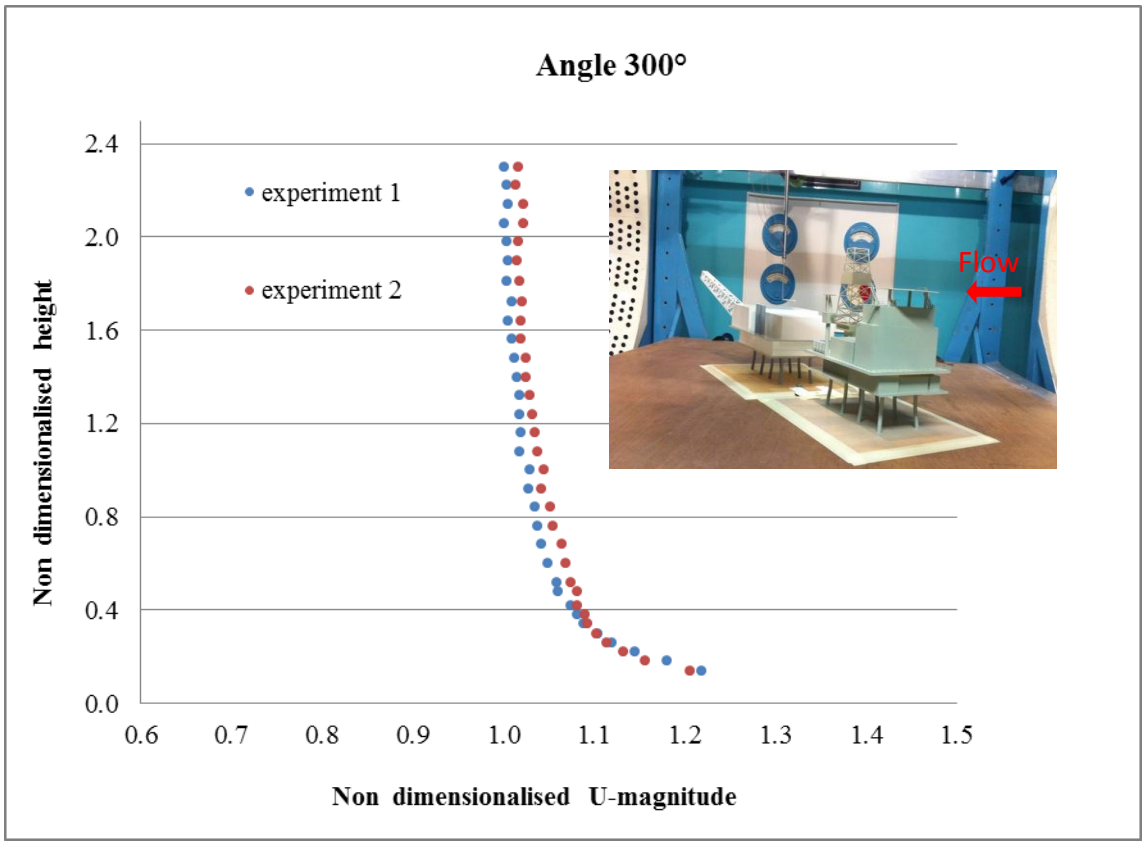

Figure 20: Velocity profile with the model in position angle 300

An undisturbed flow should be represented with a non-dimensionalised U-magnitude of 1. Therefore, in this case, the flow above the rig was distorted up to around 1.6 times the height of the platform (or 64 m height in real scale from the top of the platform).

Wind tunnel data for the other positions are reported in part 4.1.1 together with the corresponding CFD data.

2.5.2 Velocity profile around Berlengas Island

Velocity measurements were taken on a vertical line above the model using the 3D hot wire probe mounted in a right angle probe support aligned with the centre line of the wind tunnel. The origin of the island coordinate system (*x*, y, *z*) was taken at the highest point of the island (7.8 cm height) where the velocities were measured by the LiDAR. In this coordinate system the *x*-axis and *u*-component of the velocity vector were always parallel with the undisturbed free stream direction. The hot wire was moved in the vertical positive *z*-direction above the island in steps of 2cm up to 50cm above the island in the direction as shown in Figure 21. The model was rotated around the origin of the island coordinate system (*x*, *y*, *z*) every 30 degrees and velocity measurements were taken on the same vertical line for 12 different positions. The reference height used to normalise the height data was 7.8cm. This was the height from sea level of the island. The wind speed of the wind tunnel was recorded upstream by probe P11 and this data was used to normalise the velocity measurements.

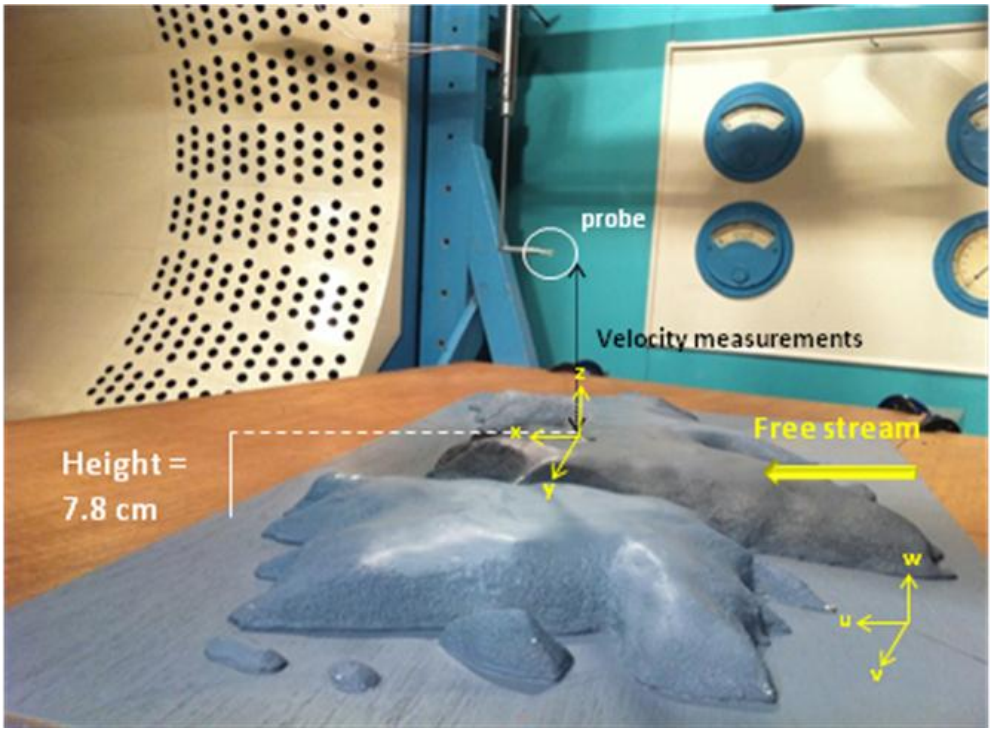

Figure 21: Berlengas island model in the wind tunnel

Velocity measurements on the same vertical line were first taken without the model to make sure the readings between the reference probe upstream and the 3D probe were in good agreement. Figure 22 shows the ratio of the readings between the two probes P91 and P11 recorded before a first run.

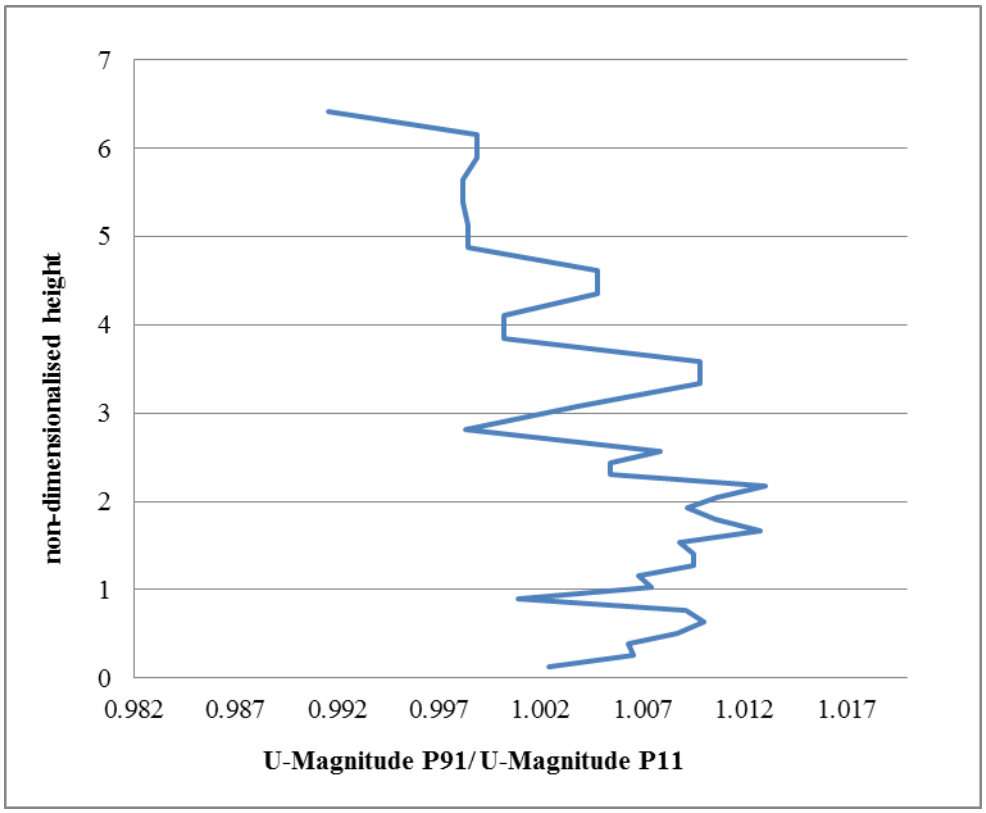

Figure 22: Measurements of the undisturbed flow for Berlengas island; Ratio of readings P91/P11

With a ratio varying from 0.992 to 1.012, the maximum difference in readings between the two probes represents 1.2% in the most extreme case. This experiment was repeated prior to each run and the difference in readings did not exceed 0.5% on average. It was concluded that this difference was sufficiently small not to be taken into account. Therefore, the direct ratio of the reading between the probe P91 / P11 would represent the non-dimensionalised data.

Velocity profiles were recorded on a vertical line with the model positioned in the wind tunnel at 12 different positions. Four of these positions are represented in the figure 23 below with the position of the vertical located as a pink dot.

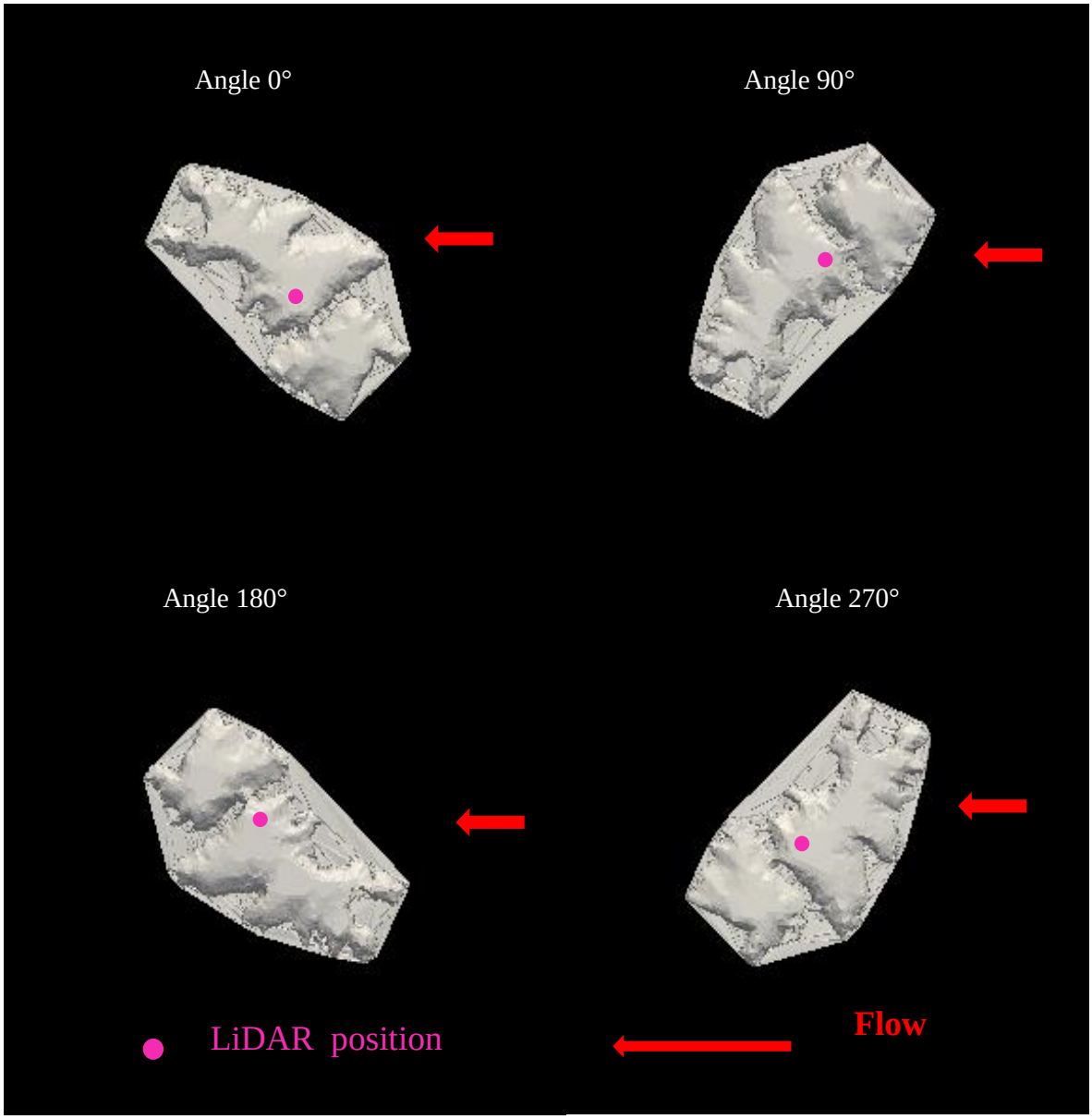

Figure 23: position of the Berlengas model

The velocity profile recorded when the model was in the position referenced as angle 0^o is presented Figure 24. The non-dimensionalised U-magnitude is shown on the *x*-axis whereas the non-dimensionalised height is on the *y*-axis. The velocity measurements on a vertical line above the island for this position were recorded

twice. Run 1 and Run 2 represent two experiments carried out at different times of the day. The profiles for these two runs are similar and confirm the consistency of the measurements.

.

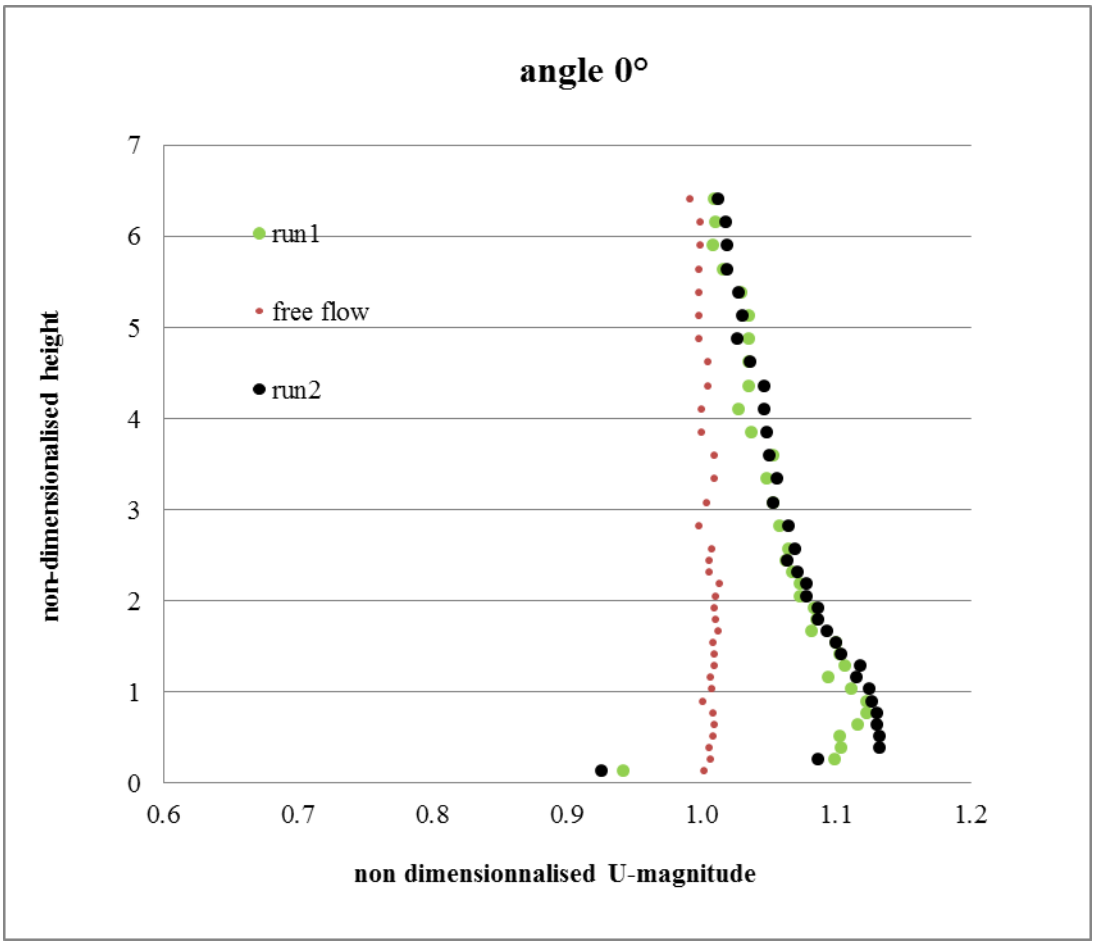

Figure 24: Velocity profile for the Berlengas island angle 0^{o}

The velocity measurements on the same vertical line when the model was not present in the wind tunnel are also reported on the graph as red dots. Any points out with these red dots represent an area where the flow was distorted by the model.

In this case, the flow was distorted up to approximately 6 times the height of the island. All wind tunnel data for the Berlingas model are reported in the part 4.2.2 together with the equivalent CFD data.

2.5.3 Velocity data around the Fino3 Mast

To measure the flow around the Fino3 mast model, the omnidirectional probe R49 was employed. This probe can measure velocities of a flow field independent of the flow direction. The probe was attached to the model at the end of the boom and the model was rotated around his centre to simulate the wind coming from different directions. The probe and the Fino3 mast model in the wind tunnel are shown below in Figure 25.

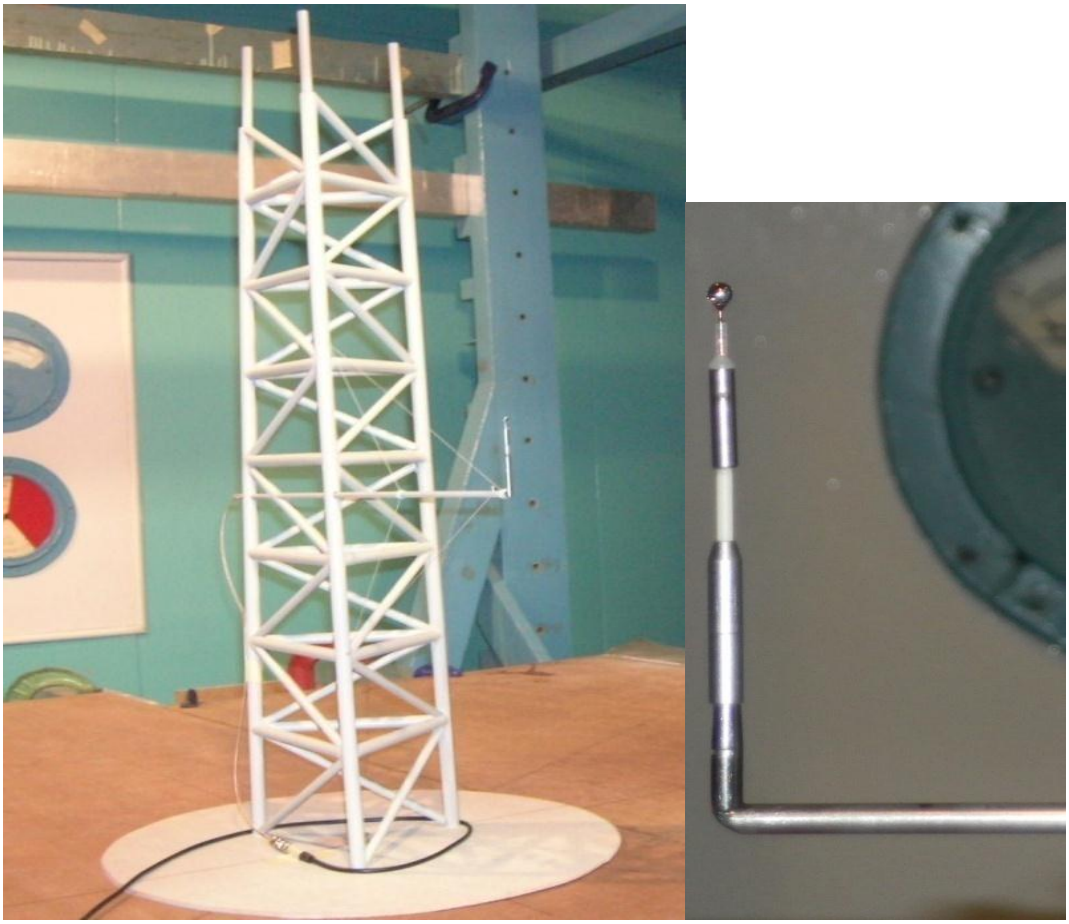

Figure 25: Probe R49 attached to the model

Velocity measurements were taken at every 30 degree angle of rotation. Figure 26 represents a view from the top of the model in 2 different positions.

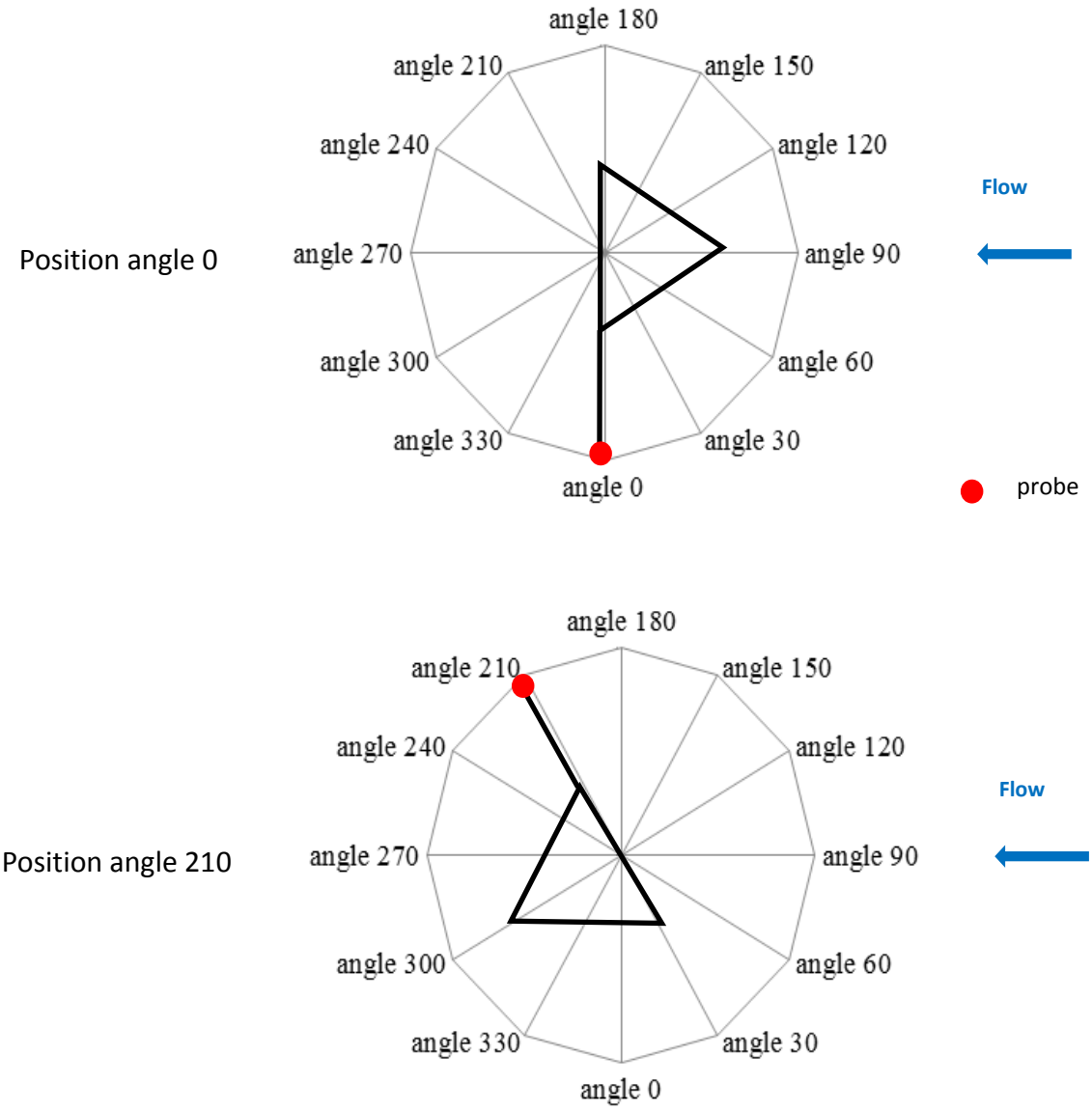

Figure 26: Position of the mast in the wind tunnel, vertical view point

The reference velocity was recorded upstream by the probe P11 in the undisturbed flow field once again to normalise the wind tunnel data. The response of the R49 probe was compared to the response of the P11 probe by taking measurements in the

empty wind tunnel. The probe R49 was attached to a support which allowed the probe to rotate around the centre of the wind tunnel as indicated in Figure 27.

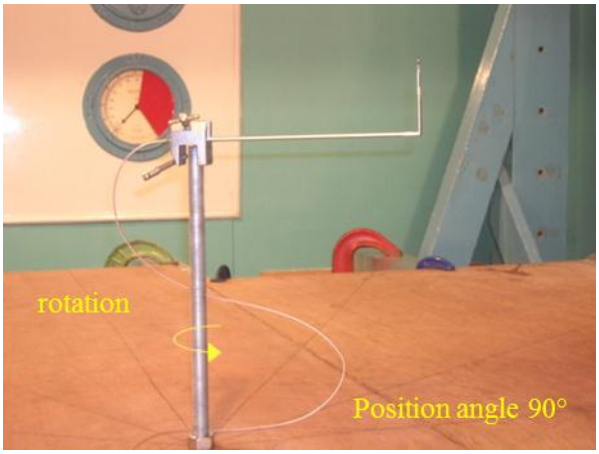

Figure 27: Measurements of the undisturbed flow with R49 probe

Velocity measurements were taken at every 30 degrees angle and the experiment was repeated twice to check the repeatability of the results. Runs 1 and 2 were performed at different times of the day and the chart shown in Figure 28 reports the ratio between the velocity measurements of probe R49 and the velocity measurements of probe P11 ($U_{point}/U_{reference}$) for the 12 different positions.

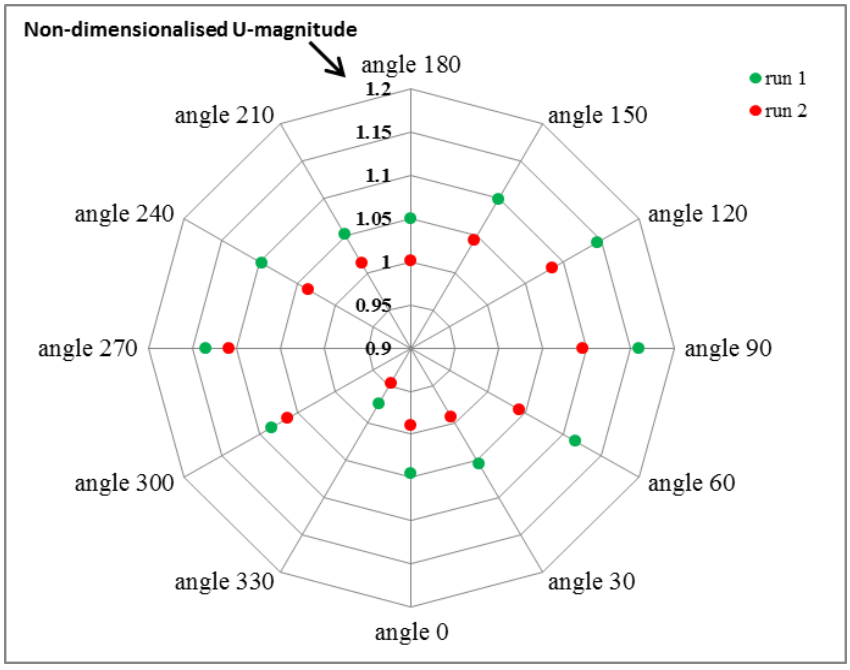

Figure 28: Repeatability trial for probe R49: ratio R49/P11

The radar chart shows the repeatability by comparing data from runs 1 and 2 for each different position. The large difference in the readings was observed when the probe was at position angle 90^o or angle 240^o. In these particular cases, the repeatability was ±3% which is in excess of the repeatability of ±0.5% found when using the probe P91 in the experiment involving the Beatrice platform. The graph can also assess the variations in U-magnitude measurements with a change in flow direction. The highest variation was seen between the position angle 90^o and angle 330^o with a difference approaching ±7%. The non-repeatability of the probe R49 was probably due to temperature effect.

These variations were considered to be significant and it was necessary to correct the data with a correction factor "CF" which takes into account the repeatability in the measurements and the differences in the data as a function the flow direction.

Two sets of measurements called "blank1" and "blank2" were carried out with the probe R49 rotating every 30 degrees in an empty wind tunnel. Between these two sets of experiments, measurements were taken with the model in the tunnel.

The correction factor for the position angle 0^o was calculated in the following manner:

$$CF(angle\ 0) = \left[\left(\frac{U_{point_1}}{U_{reference_1}} + \frac{U_{point_2}}{U_{reference_2}}\right)/2\right]_{empty\ tunnel} \qquad \text{equation 3}$$

U_{point1} is the U-magnitude measured with the probe R49 in blank1

$U_{reference1}$ is the U-magnitude measured with the reference probe P11 in blank1

U_{point2} is the U- magnitude measured with the probe R49 in blank2

$U_{reference2}$ is the U-magnitude measured with the reference probe P11 in blank2

To non-dimensionalise the wind speed measured at a specific angle with the model in the wind tunnel, the following equation was used:

$$U_{non-dim}\ (angle\ 0) = \frac{U_{point}}{CF(angle0) * U_{reference}} \qquad \text{equation 4}$$

U_{point} :*U*-magnitude measured by the probe R49 attached to the model

$U_{reference}$:*U*-magnitude measured by the reference probe P11 upstream

The figure 29 represents the non-dimensionalised U-magnitude measured around the mast. A value of U-magnitude of 1 represents an undisturbed flow. Any points away from the value of 1 mean that the flow was disturbed by the structure of the mast.

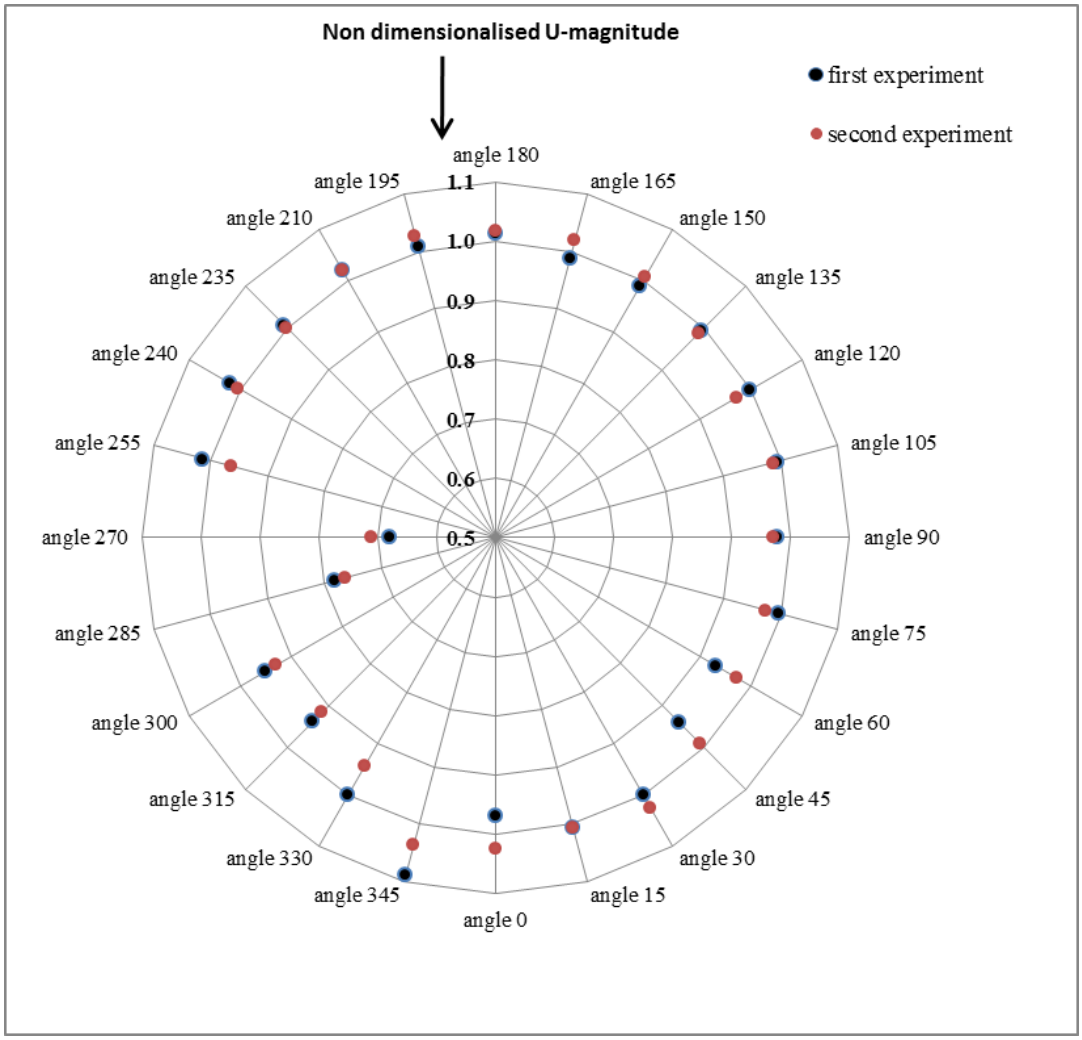

Figure 29: Non-dimensionalised velocity data around the Fino3 mast model

As can be seen in figure 29, the flow was distorted in the anticipated manner between the angles of 255^{o} to 330^{o}. These positions highlight the influence of the mast structure on the anemometer measurement location.

Two set of measurements were undertaken two days apart. The repeatability appeared to be reasonable apart from the positions at angles 0^{o}, 45^{o}, 60^{o}, 255^{o} and 345^{o} where the variation in measurements reached a value of on average ±2.5%.

When working on the Beatrice model, the probe P91 gave a repeatability of 0.5%. Therefore, it was decided to repeat the flow measurements around the mast using the P91 probe. The probe was attached to a traverse and positioned above the boom immediately in the vicinity where the probe R49 was set up, as shown in Figure 30.

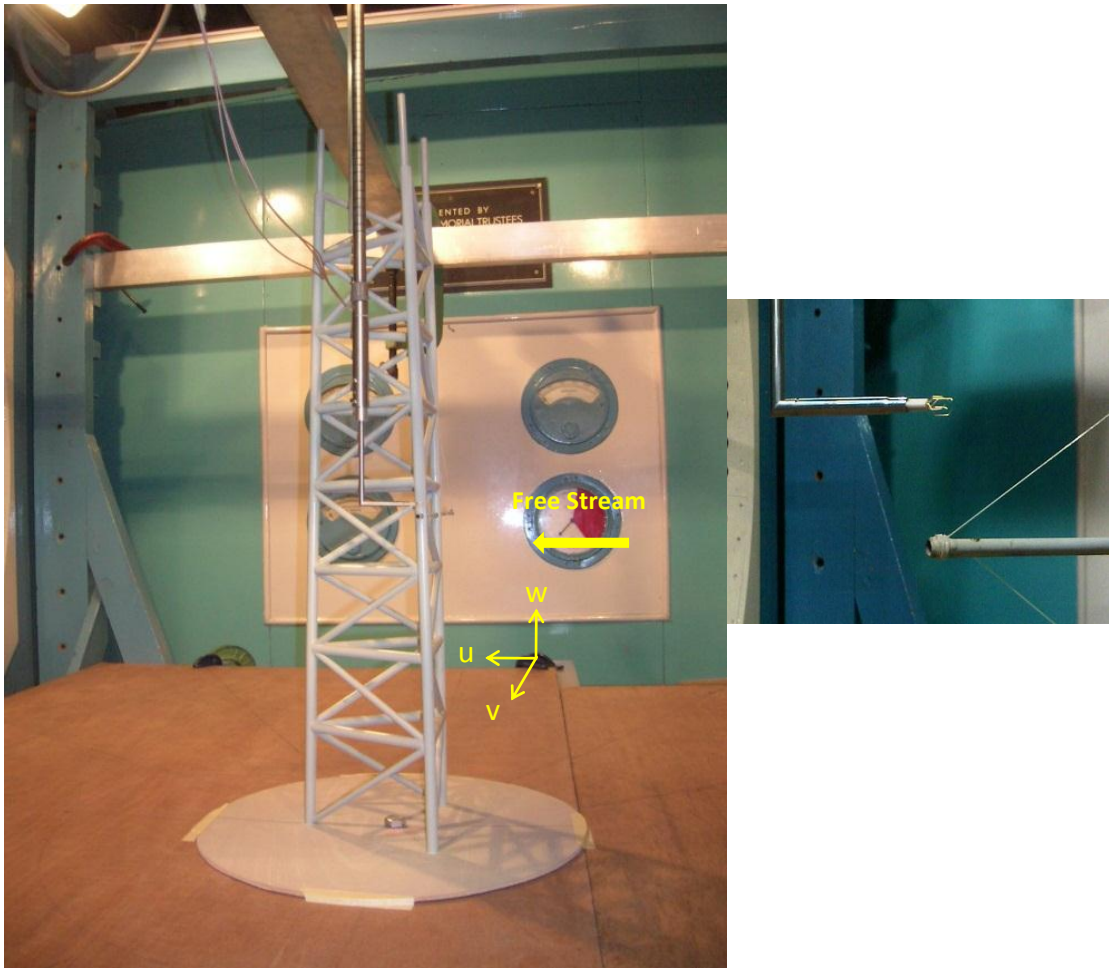

Figure 30: P91 position near the Fino3 mast model in the wind tunnel

The model was rotated around its centre and the probe P91 was positioned above the boom for each specific angle. The U-component of the velocity vector was always parallel with the undisturbed free stream direction.

The data was non-dimensionalised in the similar manner as probe R49 and this data is shown in figure 31.

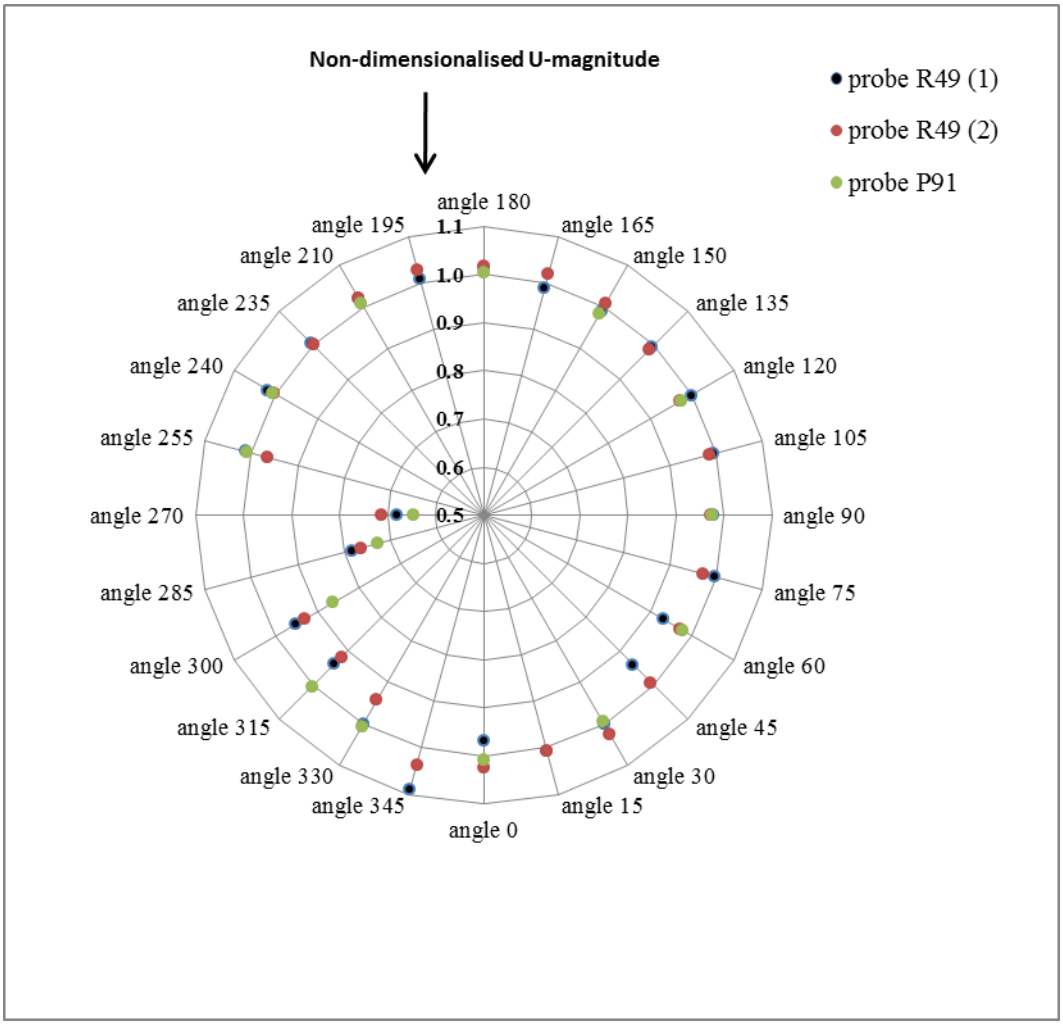

Figure 31: Non-dimensionalised velocity data around the Fino3 mast model; Measurements with probe R49 and probe P91

The data collected with the P91 probe showed good agreement with the data obtained with the R49 probe. Important flow distortion effects were observed when the model was between the position angles 255^{o} to 330^{o}. For the other positions, the flow distortion effects were very small.

Angle 90^{o} was an interesting position as the boom faces the direction of the flow and it was expected to see little distortion effects. However, the measurements carried out with both the P91 and R49 probes showed a non-dimensionalised U-magnitude of 0.98. This would suggest that the mast was providing a blockage effect upstream of

its measurement position. Measurements along the boom was taken with the P91 probe when the mast is in position angle 90 ^{o} and angle 0 ^{o} . Data are reported in figure 32a and 32b.

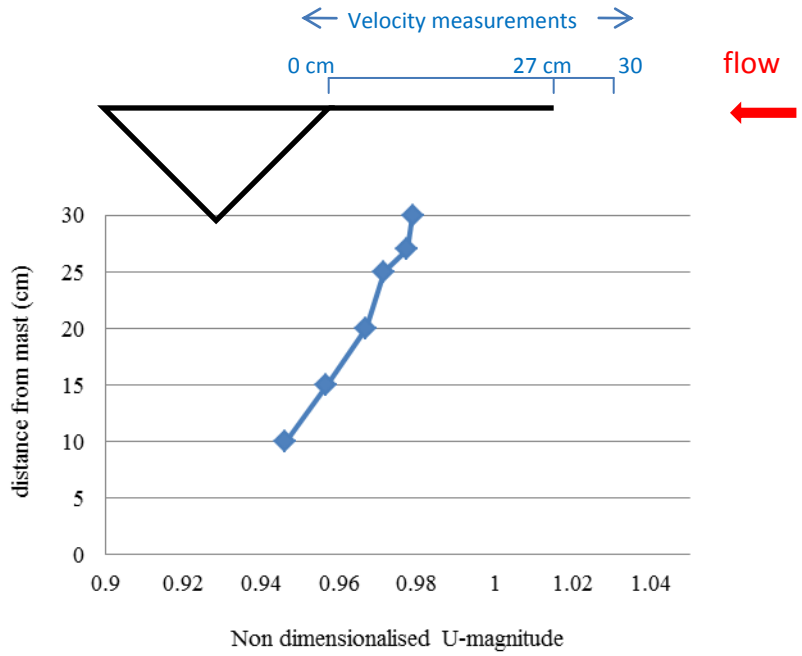

Figure 32a: Non-dimensionalised velocity data along the boom for position angle 90

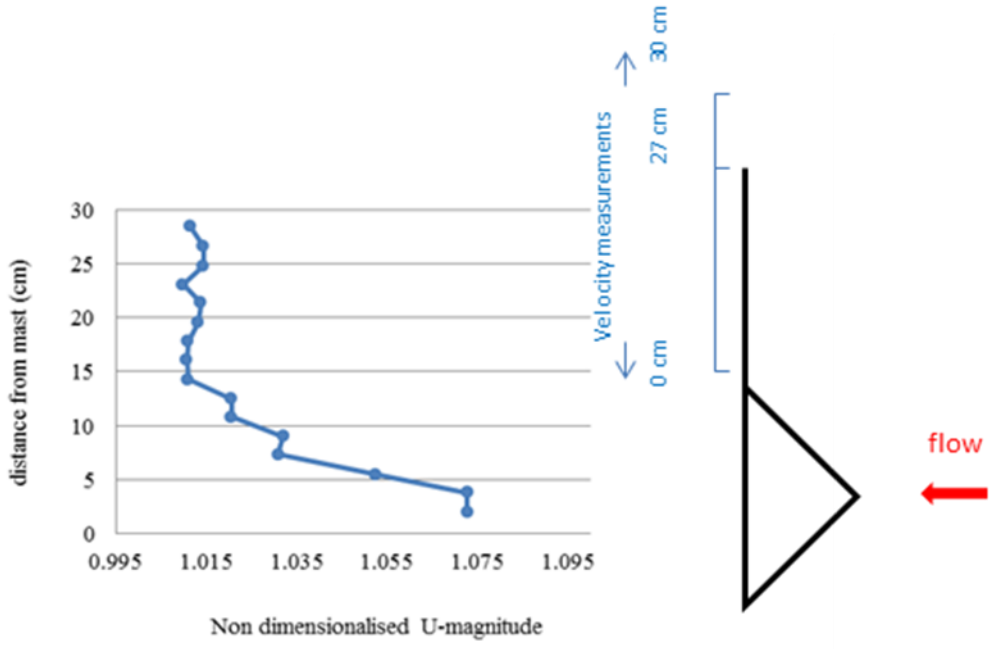

Figure 32b: Non-dimensionalised velocity data along the boom for position angle 0

The data confirmed the mast , when in position angle 90^o , had an effect on the flow up to 25 cm upstream (5m in real scale). Therefore, it is important to emphasise that the length of the boom should be greater than 5m in order to make sure the anemometer will measure an undistorted flow.

When the boom was perpendicular to the flow or in position angle 0^o , a flow distortion effect was observed up to 15 cm from the mast (3 m in real scale).

3. COMPUTATIONAL FLUID DYNAMICS MODELLING WITH OPENFOAM

3.1 OpenFOAM introduction

OpenFOAM (Open Field of Operation and manipulation) is an open source computational fluid dynamics program produced by OpenCFD Ltd. It was released in 2004 under the GNU General Public license. The software requires the use of Linux OS. Ubuntu is the version of Linux used in this study.

OpenFOAM is written in C++ and it is constituted by libraries offering core capabilities used to develop applications. OpenFOAM is distributed with a large set of precompiled applications but users also have the freedom to create their own or modify existing ones. Applications are split into two main categories: solvers and utilities.

The solvers perform the actual calculation to solve a specific problem while utilities are used to perform simple pre- and post- processing tasks such as preparing the mesh, setting up the simulation case and processing the results.

3.1.1 Equations

The principal equations solved in this study are for steady, incompressible flow the instantaneous continuity, momentum (*Navier-Stokes*) and scalar transport equations may be written in the following Cartesian tensor form:

Continuity $$\frac{\partial U_i}{\partial x_i} = 0$$ equation 5

Instantaneous Momentum Transport

$$\frac{\partial(\rho U_i U_j)}{\partial x_j} = -\frac{\partial P}{\partial x_i} + \frac{\partial}{\partial x_j}\left\{\mu_l\left(\frac{\partial U_i}{\partial x_j} + \frac{\partial U_j}{\partial x_i}\right)\right\}$$ equation 6

Applying normal Reynolds decomposition with $U_i = \overline{U}_i + u_i'$ and $\phi_i = \overline{\phi}_i + \varphi_i'$ and time-averaging the Reynolds-averaged mean flow equations may be written in the following Cartesian tensor form:

Continuity $$\frac{\partial \overline{U}_i}{\partial x_j} = 0 \qquad \text{equation 7}$$

Mean Momentum Transport

$$\frac{\partial(\rho \overline{U}_i \overline{U}_j)}{\partial x_j} = -\frac{\partial \overline{P}}{\partial x_i} + \frac{\partial}{\partial x_j}\left\{\mu_l\left(\frac{\partial \overline{U}_i}{\partial x_j} + \frac{\partial \overline{U}_j}{\partial x_i}\right) - \rho\overline{u_i' u_j'}\right\} \qquad \text{equation 8}$$

One approach to solving equation 7 and 8 is the Semi Implicit Method for Pressure Linked Equation (SIMPLE) algorithm [23]. In this method, an approximate velocity field is obtained by solving the momentum equation with an old pressure. The pressure term is calculated using equation 8 and the latest velocity information.
This algorithm is implemented in OpenFOAM and was used to solve the problem.

3.1.2 Process

The CFD modelling of a flow around a model followed a same basic procedure which can be divided into three steps: pre- processing, solving and post- processing.
During the pre- processing stage, the physical bounds of the problem was defined. The volume occupied by the fluid was divided into discrete cells to form a mesh. The physical modelling and the boundaries conditions were defined.
The simulation was started and the equations was solved using a precompiled simple potential flow solver PotentialFoam. The potentialFoam solver solved equations describing the conservation of mass and momentum. The resulting inviscid flow field was then used to provide the initial conditions for the resulting viscous, turbulent solution using the simpleFoam solver. This solution technique could significantly improve the solubility of the solution and promote rapid convergence. Convergence was achieved when the global sum of residuals fell below a small value, typically 10^{-5}.

3.1.3 Conditions specification

The purpose of our work was to simulate the flow around the wind tunnel models (Beatrice platform, Berlengas Island and Fino mast) with flow conditions based on the wind tunnel experiment.

The geometry of the model was supplied as a .stl format which is a standard output format from any CAD package. The CAD drawings were created with a geometry representing the models used in the experimental work. The stl geometries for the 3 models are shown in appendix .

The inlet flow velocity was U=15m/s and the Reynolds number was as follow:

- For the Beatrice platform case: $Re = U L / \nu = 15 \times 0.5 / 1.5 \times 10^{-5} = 5 \times 10^{5}$

(U is the mean flow velocity, L is the platform lenght and ν is the dynamic viscosity of air)

- For the Berlengas island case: $Re = 15 \times 1.2 / 1.5 \times 10^{-5} = 12 \times 10^{5}$

(Where 1.5 is the length of the island in m)

-For the Fino3 mast case: $Re = 15 \times 0.01 / 1.5 \times 10^{-5} = 1 \times 10^{4}$

(Where 0.01 is roughly the diameter of the mast leg in m)

As it was expected to have a turbulent flow , turbulence modelling was therefore required. The CFD modelling problems were all steady-state and the turbulence model was one of the Reynold Averaged Stress model with standard wall-functions to determine the shear stresses at solid surfaces. The turbulence model used in these problems was the k-omegaSST model [23].

3.2 Methodology for solution

3.2.1 Pre- processing tasks

Cleaning up dirty CAD geometries

In general, ".stl" geometries from CAD packages were made from triangulated surfaces. There may be triangles duplicated, thin or not fully closed. Such triangles could cause problems during the meshing process. The OpenFOAM utilities surfaceCheck and surfaceConvert were used prior to any meshing to find these triangles and fix them.

Setting up the background mesh

The computational domain was set up to be 5L upstream from the model , 5L on each side and 5L above, with a length approximately 15L downstream (L being the length of the model). These parameters were defined in the blockMeshDict dictionary. The boundary condition types such as inlet, outlet and walls were specified in this dictionary. The back ground mesh distribution was also specified and then created using the blockMesh utility.

Grid refinement

In order to capture fine detail around the model, a refinement box with denser mesh was defined using the variable refinementBox in the snappyHexMeshDict dictionary. A level of refinement was also set up to satisfy the y^+ requirement. At wall surfaces, in order for the wall functions to work effectively, we required the non dimensional distance y^+ to be between 30 and 200.

y^+ is defined as : $y = y^+ \nu / U_*$

y is the first cell centre distance at any wall surface

$\nu = 1.5 \times 10^{-5}$ m^2/s is the laminar kinematic viscosity

U_* is the shear velocity.

For a case of turbulent flow over a plate U_* is defined as follow:

$$U_* = \sqrt{\frac{\tau_w}{\rho}} = U\sqrt{\frac{C_f}{2}} = U\sqrt{0.0359\,Re^{-0.2}}$$

equation 8

Where τ_w is the wall shear stress, ρ is the fluid density and C_f the skin friction coefficient. With a Reynolds number between $0.8.10^5$ and 8.10^5, y should be around 6 mm when possible.

Final mesh generation

The first step in the meshing process was to generate a castellated mesh. This process generated a rough mesh, which followed the outline of the surface of the .stl geometry.

The next stage was to snap the rough, castellated mesh on to the surface to produce a smooth mesh, which closely represented the model surface.

Finally, in order to improve the mesh near to the walls, boundary faces and edges were merged. The utility snappyHexMesh was used to generate such meshes.

3.2.2 Solving the problem

After completing the mesh, the problem was ready to be solved. The initial conditions and the boundary conditions for the turbulence fields were estimated from the inlet velocity U, the turbulence intensity I, the characteristic length scale of the turbulence L and the turbulence constant C_μ. In the wind tunnel, the typical value for I = 1%, L = 0.1 x the tunnel diameter = 0.15, while the inlet velocity was 15 m/s.

The turbulent kinetic energy k and the specific turbulent dissipation rate ω were recorded in the initialConditions directory as followed:

$k = 1.5\,(UxI)^2 = 1.5\,(15x0.01)^2 = 0.033\ m^2/s^2$

$\omega = C^{-0.25}k^{0.5}/L = 0.09^{-0.25}x0.033^{0.5}/0.15 = 2.2\ s^{-1}$

The potentialFoam and simpleFoam solvers were then run in the manner described in section 3.1.2 until convergence was achieved.

3.2.3 Post processing tasks.

The CFD modelling results were post-processed using two main utilities;

- SampleDict in order to obtain quantitative data.
- ParaFoam in order to visualize the data.

SampleDict

The data collected in the wind tunnel were:

- The U-magnitude of the velocity vector on a vertical line above a specific point of the model
- The U-magnitude velocity at a specific point in the case of the fino3 mast

In order to extract this information from the CFD solution, the following key entries in the sampleDict dictionary were set:

- setFormat	raw	set the output format for raw data
- fields	U	the 3 components of the velocities vectors were sampled
- type	uniform	points measurements were evenly distributed on the line
- axis	distance	sample location as the distance from the start of the sampling line
- start	(0.51 -0.085 0.25)	coordinates of the start point of the line
- end	(0.51 -0.085 3)	coordinates of the end point of the line
- nPoints	100	numbers of sampling points

The values of the three components of the velocity vector were sampled from the simulation and written to a file by using the command sample -latestTime. The U magnitude was calculated from the three U components and the data were non-dimensionalised using the inlet velocity of the simulation (15m/s) as a reference. The CFD data were then compared with the experimental data.

In the case of the mast where only point measurements were recorded during the experiments in the wind tunnel, the values of the 3 components for the velocity were sampled from the simulation on the line situated above the boom. The velocity values at the end of the boom were extracted from the data.

ParaFoam

The main post-processing tool provided with OpenFoam is called paraView, an open-source 3D scientific visualization application. The utility paraFoam allows this application to be launched. ParaFoam allows the user:

- To check the quality of the mesh in the pre-processing step
- To visualise the model and define the position of the vertical line where the measurements were taken in the wind tunnel experiment.
- To display the vector fields and contours of velocity.

3.3 CFD modelling description

This section describes in details the CFD modelling for three models. Separate meshes were created for each of the other 12 flow directions considered by rotating the model to the appropriate angle of incidence and the problem was solved for each of the meshes. Only one case representing the model in position angle 0 is reported below as the procedure for the modelling was similar from one angle to the other.

3.3.1 Description for Beatrice Platform case

Pre-processing

With the model dimensions being 1.3x0.5x0.5 m, the size of the computational domain was set as 9x9x3 m with the flow inlet patch located 3.8 m upstream. For the background mesh, there were 40 cells in the x-and y-directions and 30 cells in the z-direction. This means that the edge length of each computational cell with the width edge was around 0.22 m and the edge height was around 0.1 m. In the snappyHexMesh, the size of the refinement box position around the model was set up as 2x1x1.5 m with two level of refinement guaranted. With a level of refinement near the walls set up at 6, this should have produced a near wall cells with a

dimension of 0.22 / 2^6 ≈ 3.5 mm. The setting nCellsBetweenLevels, which controls the abruptness of the mesh refinement, was set as 1. Figure 33 shows the Beatrice platform geometry with the background mesh.

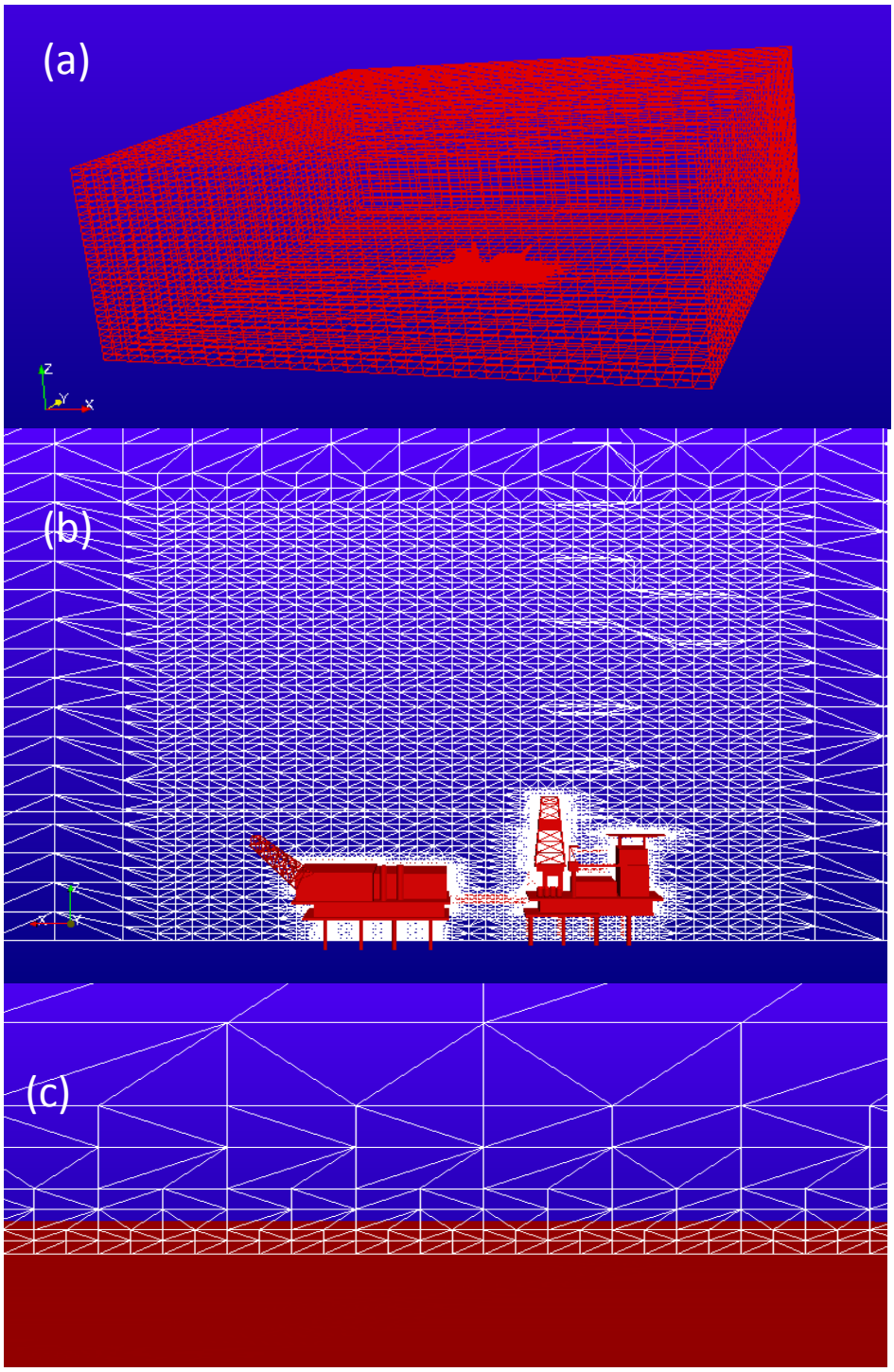

Figure 33: Beatrice platform geometry and background mesh: (a) extent of CFD domain, (b) refinement zone around rig, (c) mesh close to rig wall

The meshing process started with a castellated mesh (Figure 34), snapped at the surface. Boundary faces and edges were merged to create the final mesh represented in Figure 35. A total of 4 million cells made the final mesh for this case.

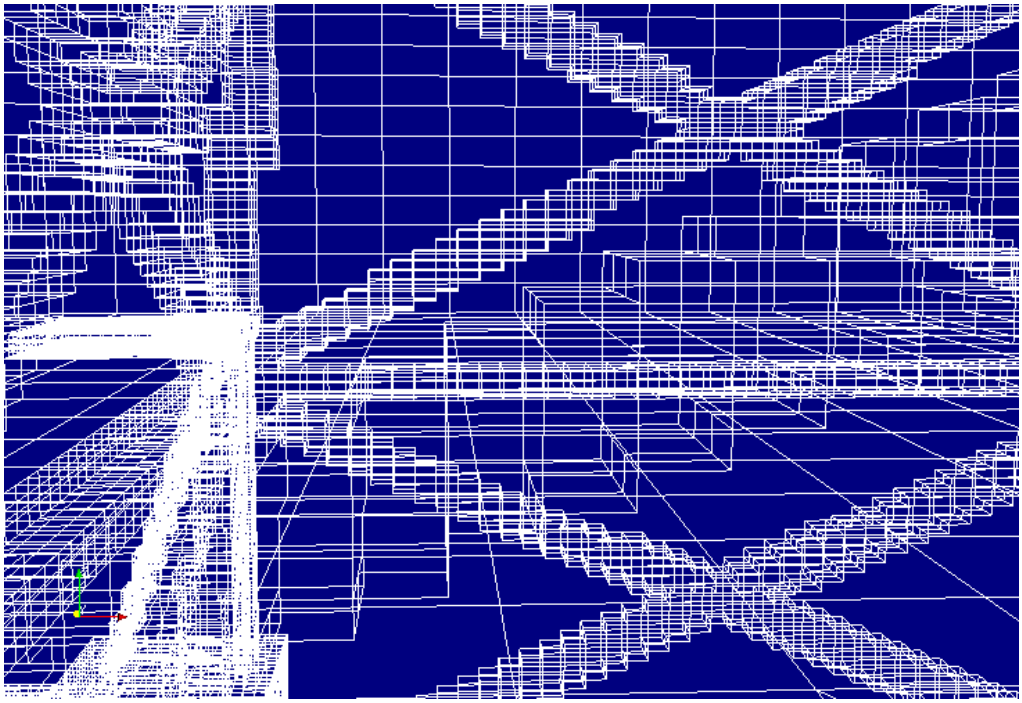

Figure 34: Castellated mesh for Beatrice

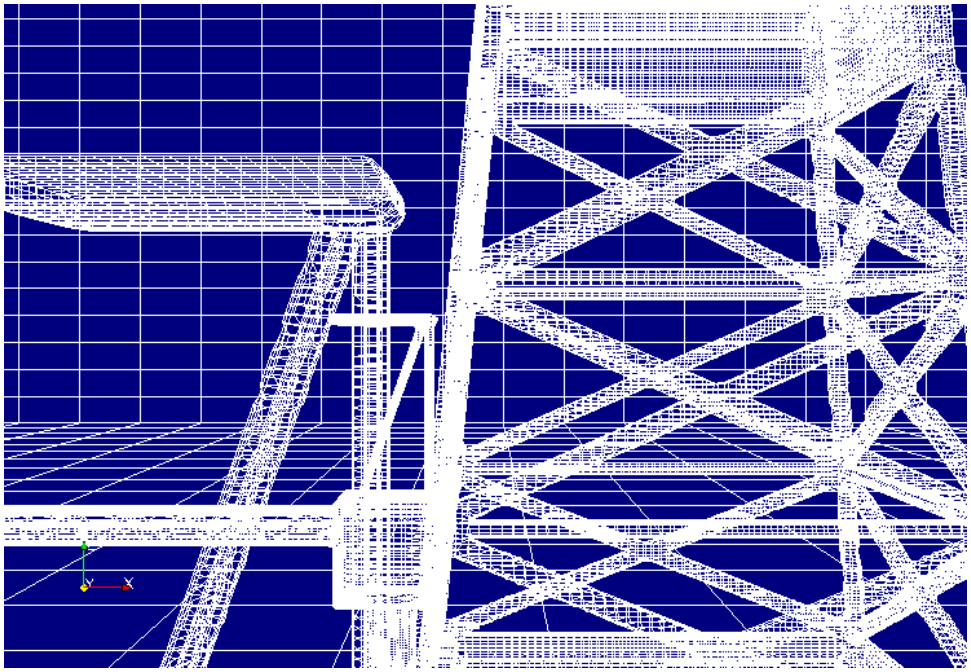

Figure 35: Surface mesh after merging cells in region of the derrick

Solving the problem

The case was solved with the boundary and initial conditions and the choice of the solver as described in section 3.4.2. During a run, the residuals of the velocity component in the y-direction were monitored. It is preferable to monitor the residuals of the velocity component which is not in the main flow direction to obtain a better indication of the degree of convergence. The open-source graphics package Gnuplot provided an output of the degree of convergence of the case. Figure 36 shows that the convergence was achieved to a level of 0.00002 in this case.

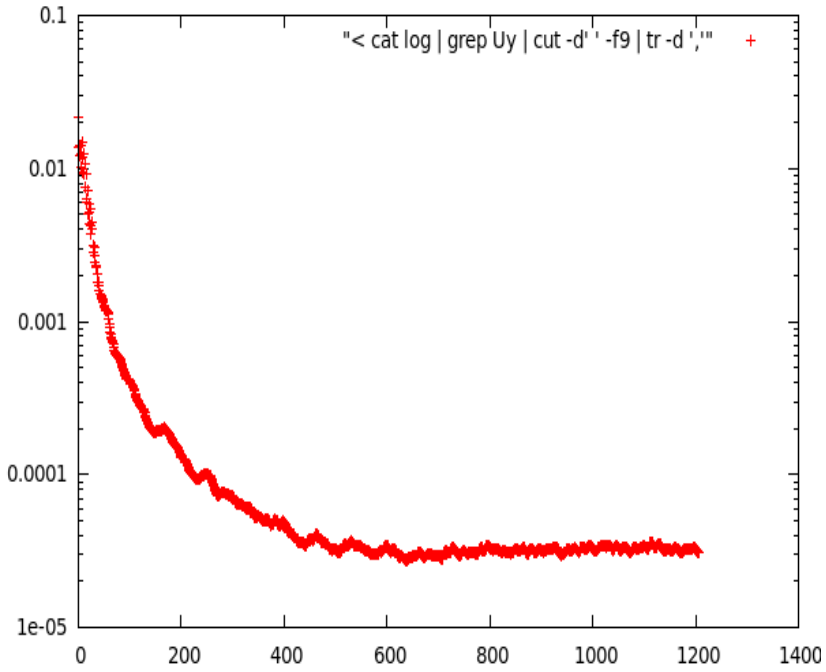

Figure 36: Gnuplot output for Uy-residuals

3.3.2 Description for Berlengas Island case

Pre-processing

The size of the computational domain was set as 3x3x1 m with a background mesh containing 60 cells in the x- and y- directions and 50 cells in the z-direction. A refinement box was set up around the model with the dimensions been 1.76x1.4x0.5 m and two level of refinement. In this case, the refinement near the wall was set up at

1 in order to limit the total number of computational cells below 2 Millions. Figure 37 illustrates the background mesh for the Berlengas Island.

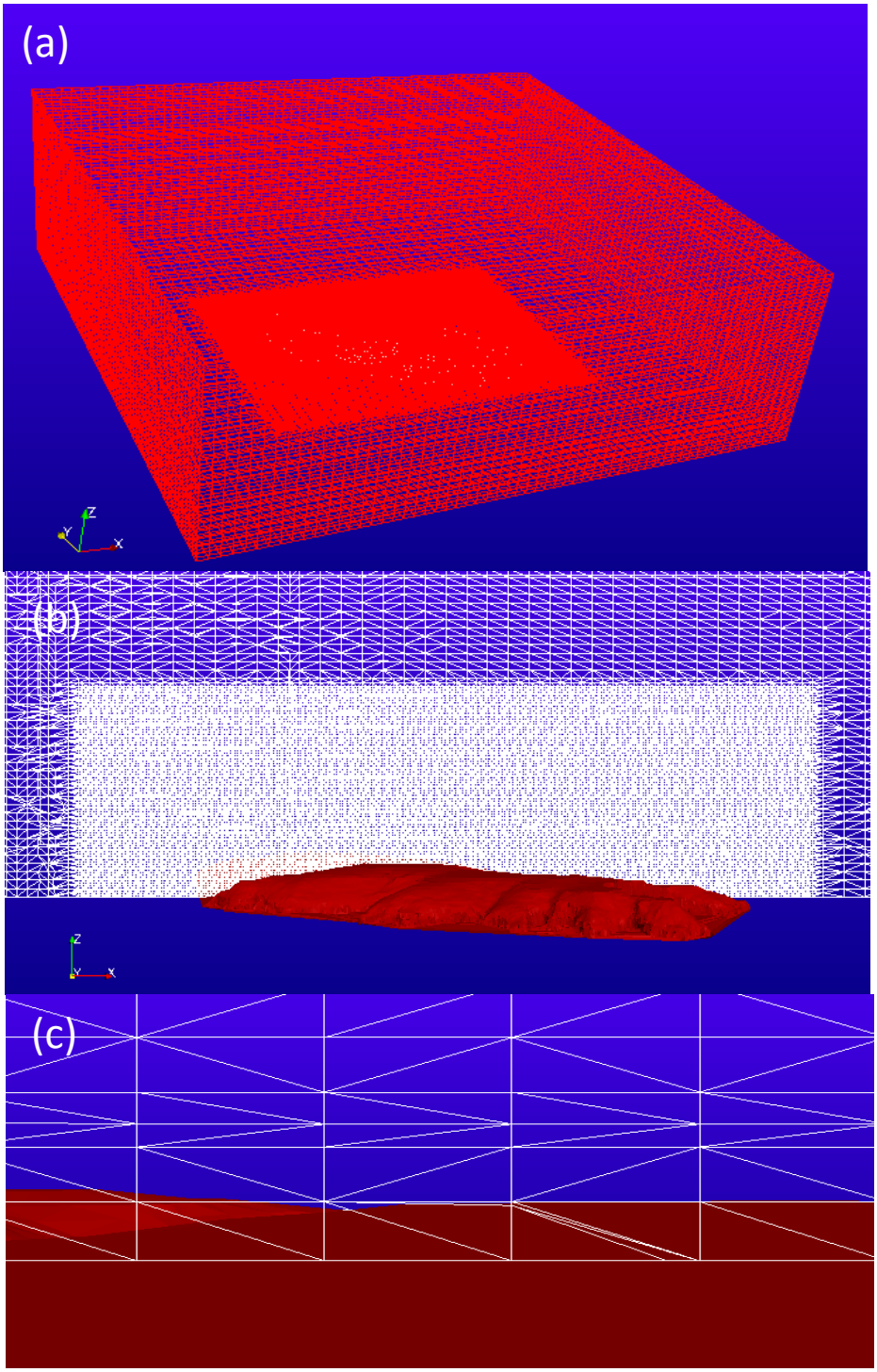

Figure 37: Berlengas island background mesh: (a) extent of CFD domain, (b) refinement zone around island, (c) mesh close to the island wall

The snappyHexMesh utility was then employed to snap the hexahedral mesh onto the surface of the island, resulting in the surface mesh shown in Figure 38.

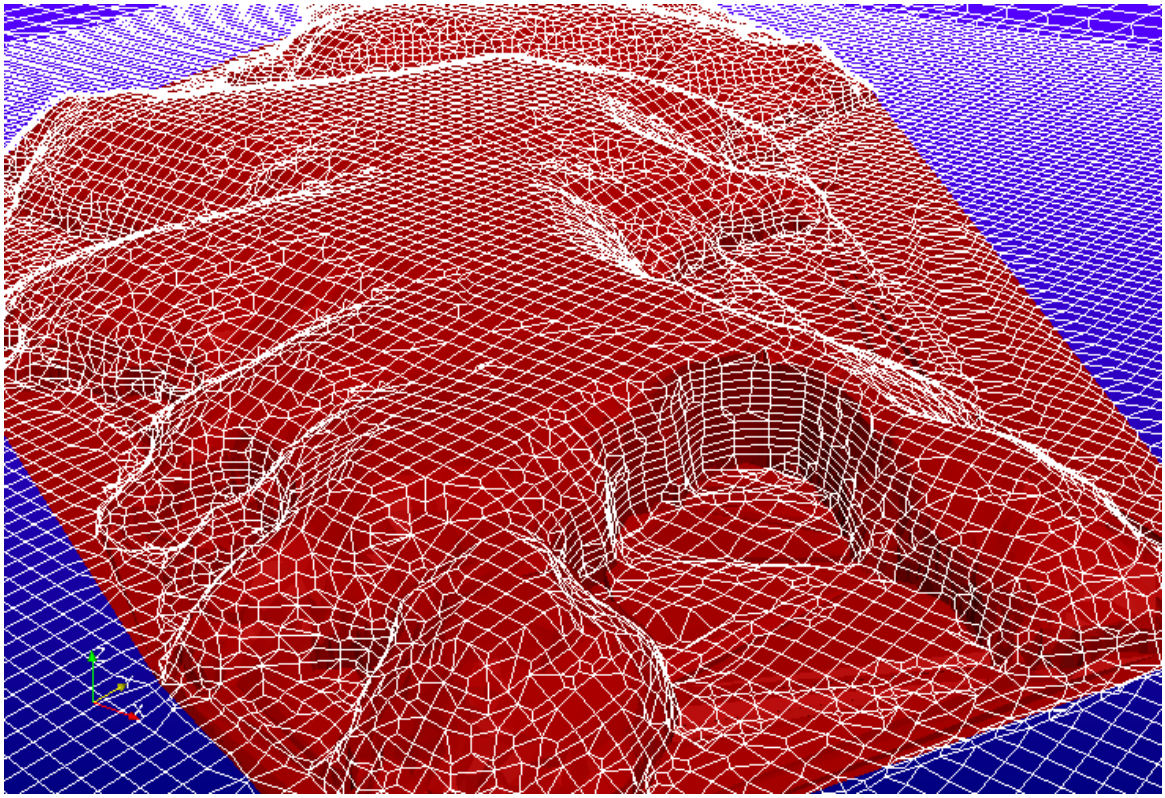

Figure 38: Snapped surface mesh on the Berlengas Island

Solving the problem

The case was solved with the boundary and initial conditions and the choice of the solver as described in section 3.4.2. Once more,during a run, the residuals of the velocity component in the y-direction were monitored . The convergence was achieved to a level of 0.004 in this case with a y+ of 120 as shown in Figure 39.

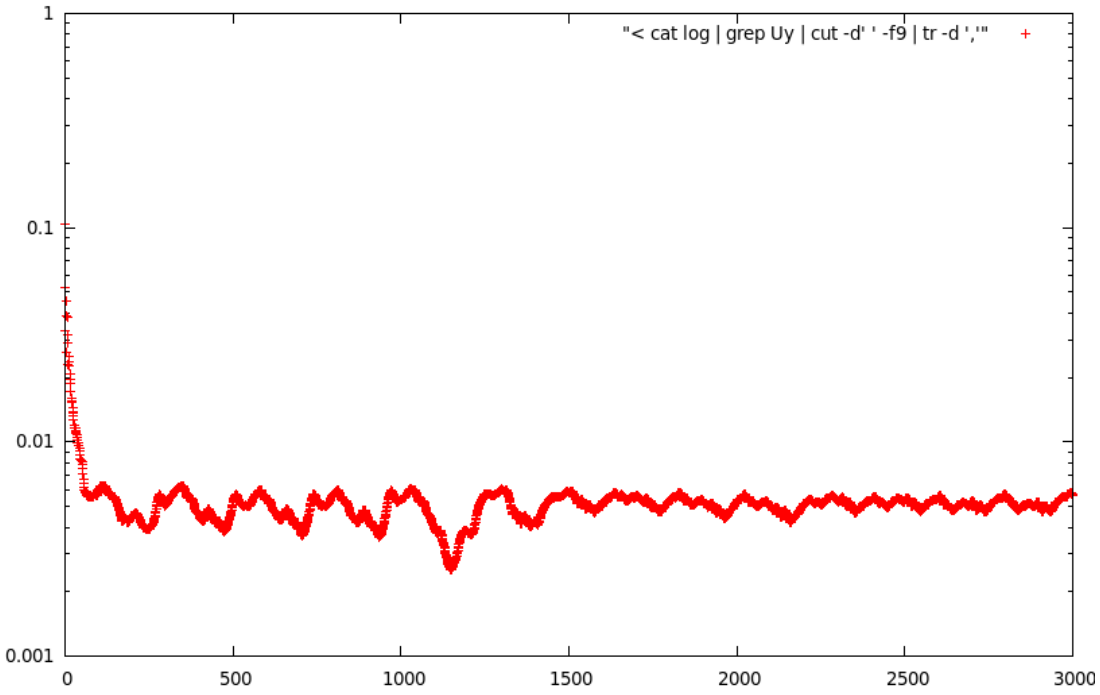

Figure 39: Gnuplot output for Uy-residuals for Berlengas Island

3.3.3 Description for Fino3 Mast case

Pre-processing

With a size of the model being 0.18x0.21x0.81 m, the computational domain dimensions were set up as 2.5x2.2x1 m. 50 cells in the x- and y-direction and 40 cells in the z-directions were introduced to form the background mesh. A refinement cylinder was created with a height of 1 m and a radius of 0.5 m. The model stood at the centre of both the computational domain and the refinement cylinder. The level of refinement was set up at 2 for the refinement region and at 3 for the refinement surface. This should have produced near wall cells with a dimension of $0.05 / 2^3 \approx 6$ mm.

The resulting background mesh is shown Figure 40.

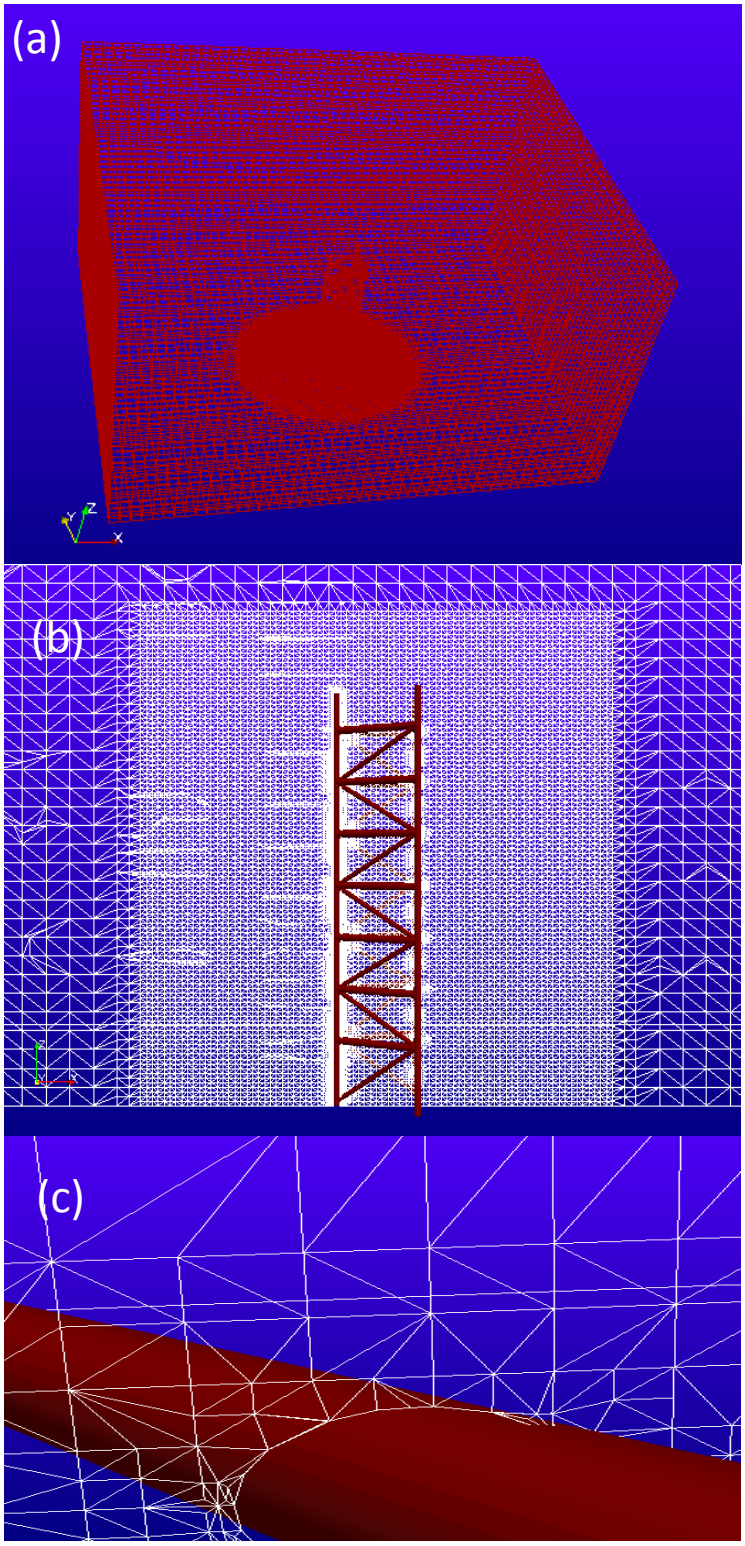

Figure 40: Fino3 mast background mesh: (a) extent of CFD domain, (b) refinement zone around mast, (c) mesh closed to the mast wall

The hexahedral mesh was snapped onto the surface of the mast. The resulting mesh consisted of around 1.5 million hexahedral and polyhedral cells around the model. The final surface mesh is shown Figure 41.

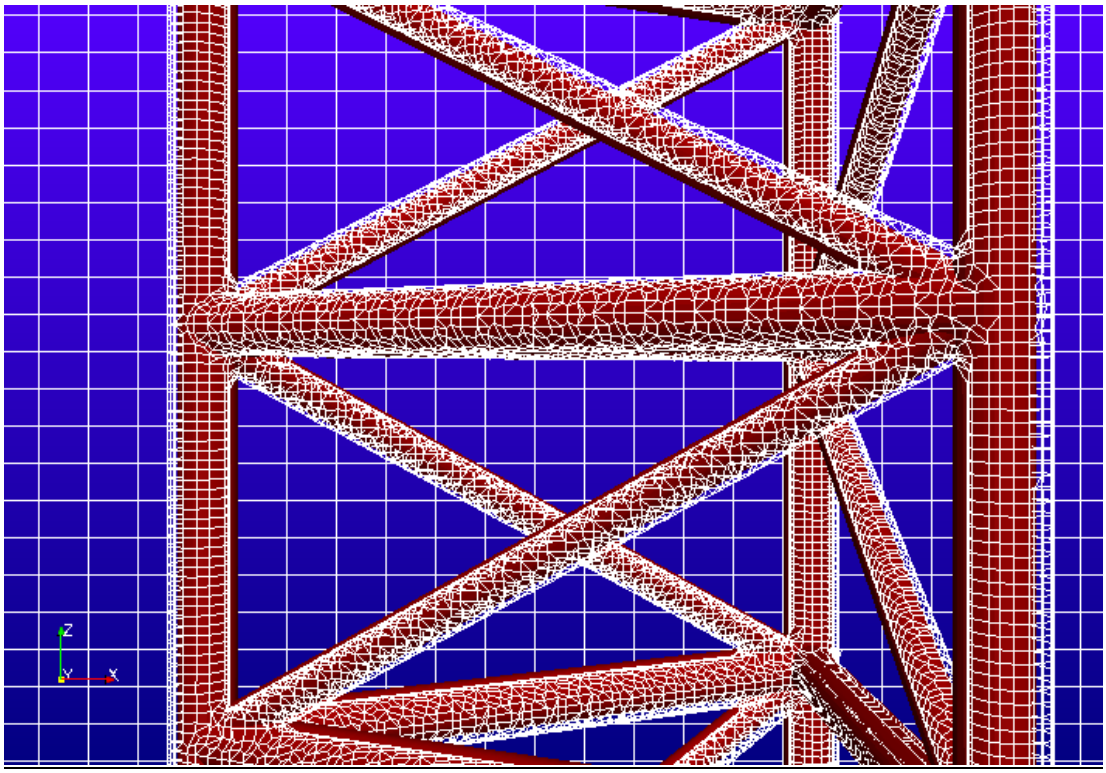

Figure 41: Snapped surface mesh on the Fino3 mast

Solving the problem

The case was solved with the same boundary and initial conditions as for the Berlengas Island case and the Beatrice platform case. The graph below shows the residuals of the velocity component in the y-direction. The convergence was achieved to a level of 0.00008 in this case with an average y+ of 32.

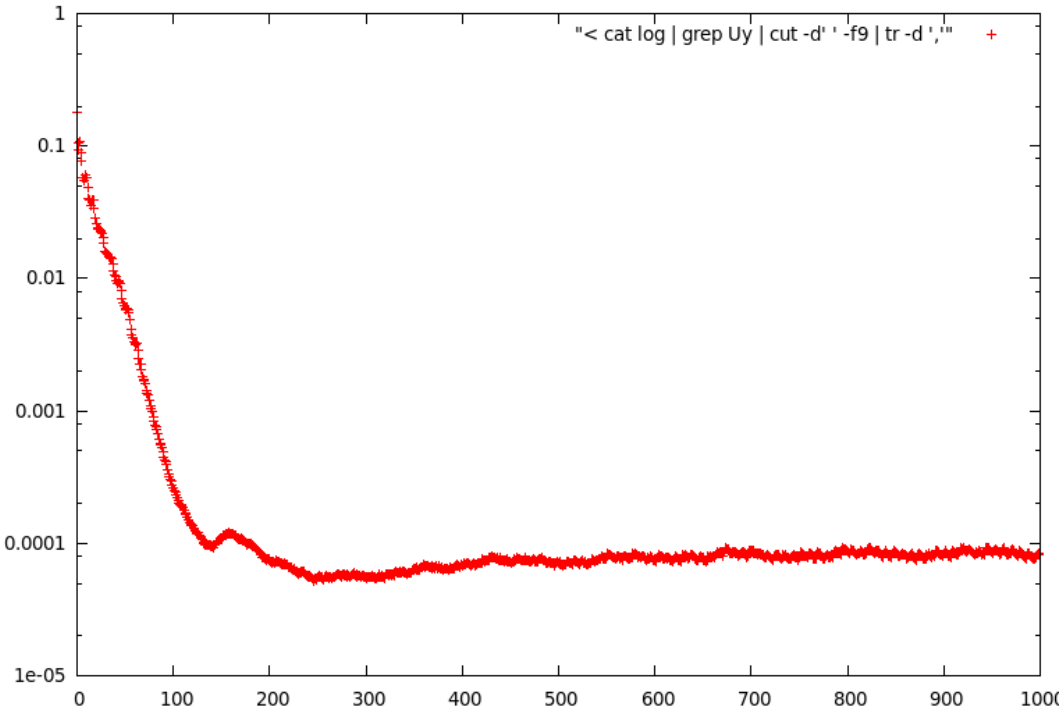

Figure 41: Gnuplot output for Uy-residuals for Fino3 mast

4. COMPUTATIONAL FLUID DYNAMICS MODELLING WITH OPENFOAM- RESULTS

In this section, experimental data are compared with the data from the CFD modelling. The velocity data from the CFD modelling were taken on the same position above the model as in the wind tunnel. This comparison will give an idea how well the open-source CFD software OpenFOAM can model the flow.

4.1 Results for Beatrice Platform

4.1.1 Velocity profile: comparison of OpenFOAM data with wind tunnel data

The OpenFOAM-predicted velocity profile for the 12 flow angles are shown in figure 42 and compared with the wind tunnel data.

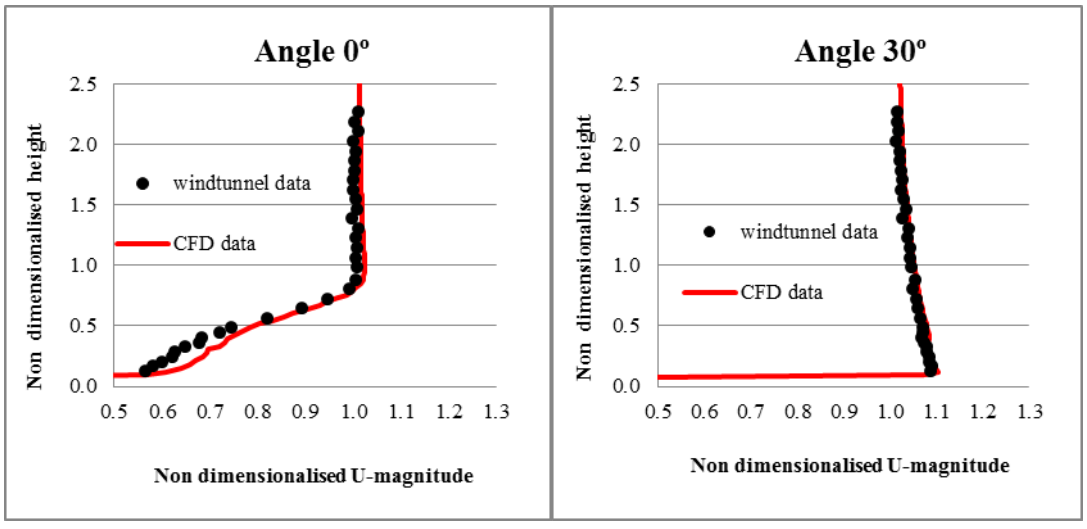

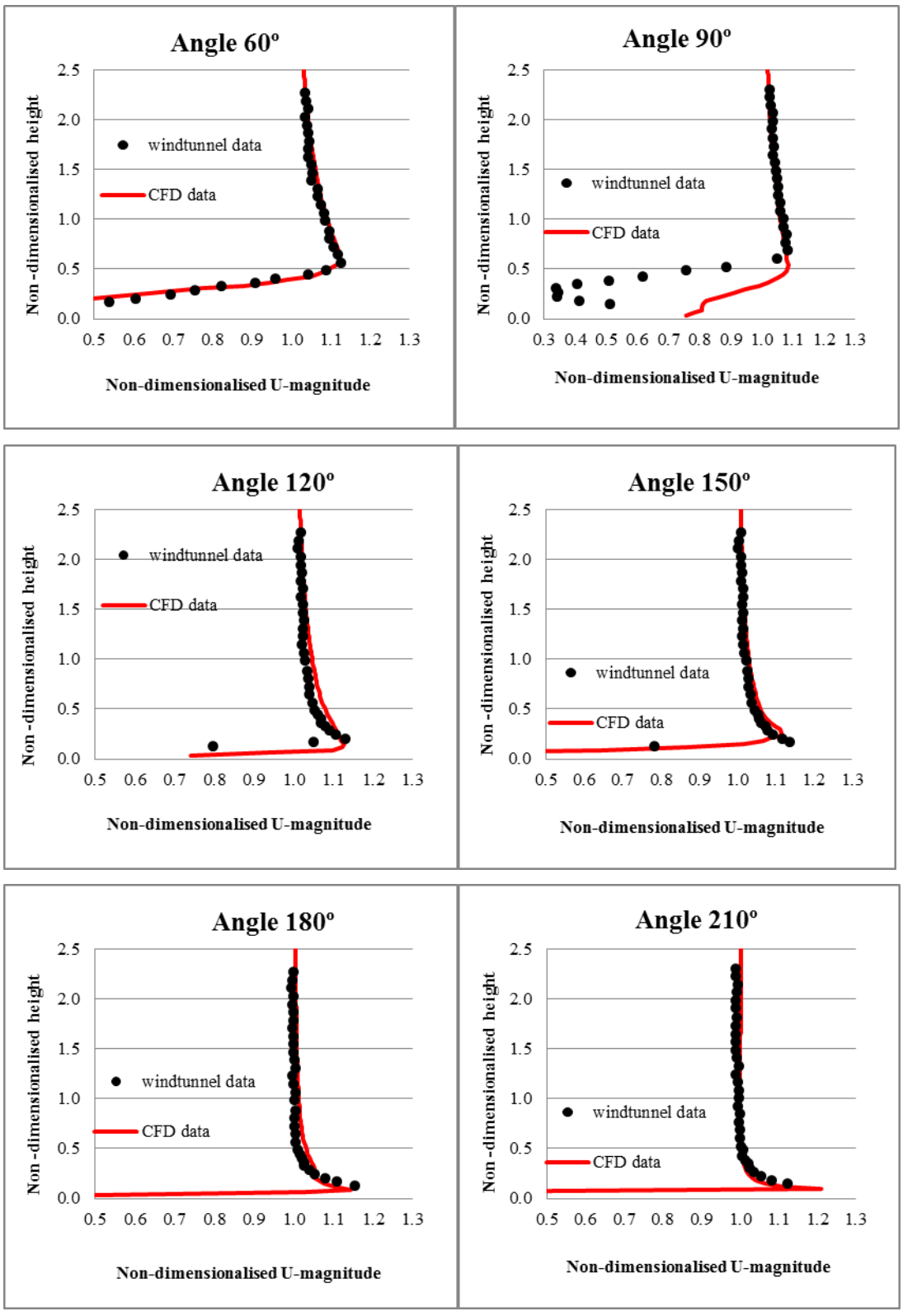
Angle 60º
Non -dimensionalised height
windtunnel data
CFD data
Non-dimensionalised U-magnitude
Angle 90º
Non -dimensionalised height
windtunnel data
CFD data
Non-dimensionalised U-magnitude
Angle 120º
Non -dimensionalised height
windtunnel data
CFD data
Non-dimensionalised U-magnitude
Angle 150º
Non -dimensionalised height
windtunnel data
CFD data
Non-dimensionalised U-magnitude
Angle 180º
Non -dimensionalised height
windtunnel data
CFD data
Non-dimensionalised U-magnitude
Angle 210º
Non -dimensionalised height
windtunnel data
CFD data
Non-dimensionalised U-magnitude

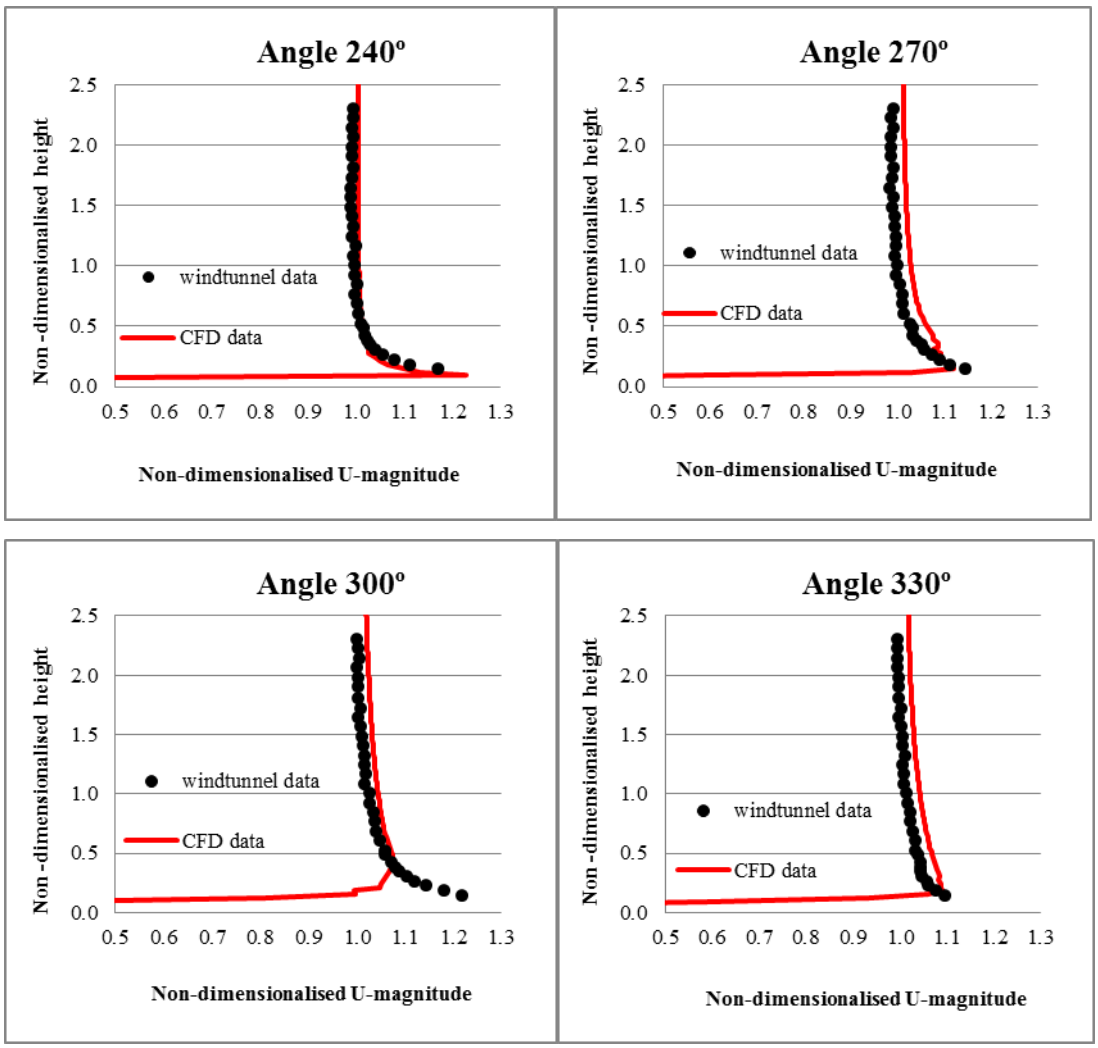

Figure 42: Comparison of velocity profile data OpenFOAM/ wind tunnel for Beatrice platform case

An acceleration or retardation velocity near the surface of the model was recorded by the experimental data in the majority of the cases. In general, the flow distortion was captured satisfactorily by the OpenFOAM simulation. Only two cases (angles 90º and 300º) showed the CFD data near the surface not concurring with the experimental data. Figure 43 shows the velocity streamlines for the position angle 90°. In this specific case, the graph shows the flow passing through the flare stack before reaching the corner of the platform where the velocities measurements were taken. The flare stack has a very complex geometry and creating a representation of the real model using CAD software was quite a challenge. Therefore, the geometry

between the model used during the experiment and the CAD model certainly contained slight differences which may have had an impact on the flow modelling.

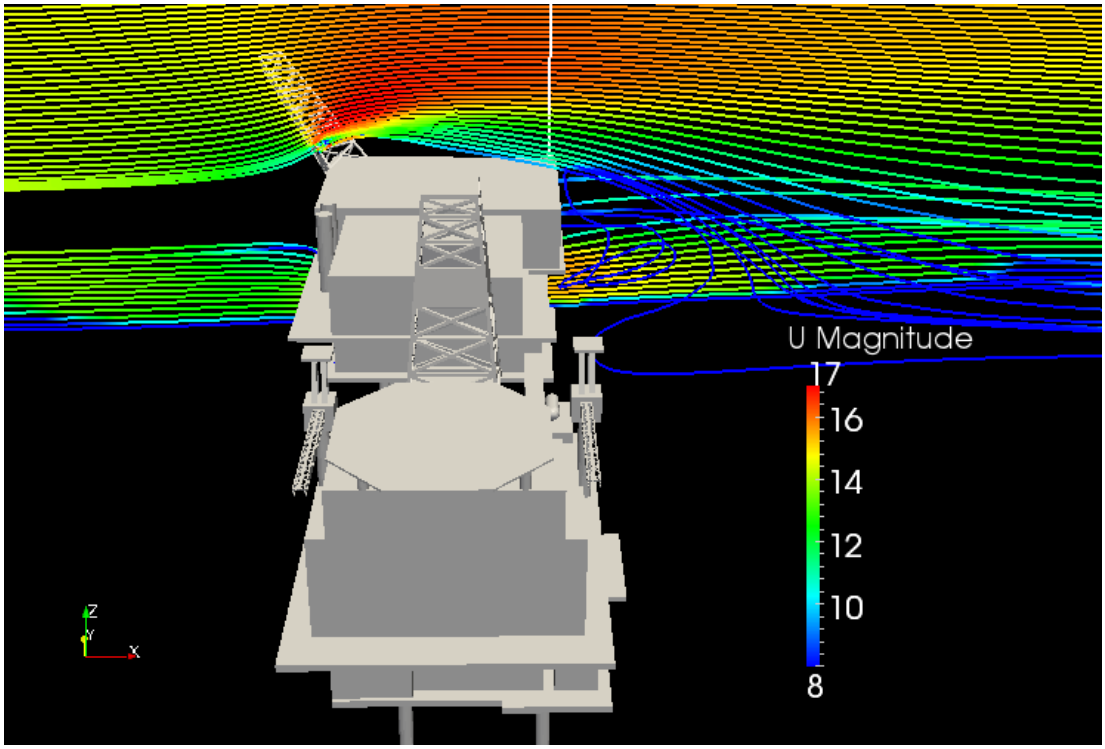

Figure 43: Velocity streamlines for Beatrice angle 90º

When the platform was in position angle 300°, the flow above the measuring point reached the corner of the platform as shown in figure 44. The flow around this rectangular blockage represents a complex turbulent zone. Such complex 3D flow features are challenging for a CFD code to capture and this is not different in this case.

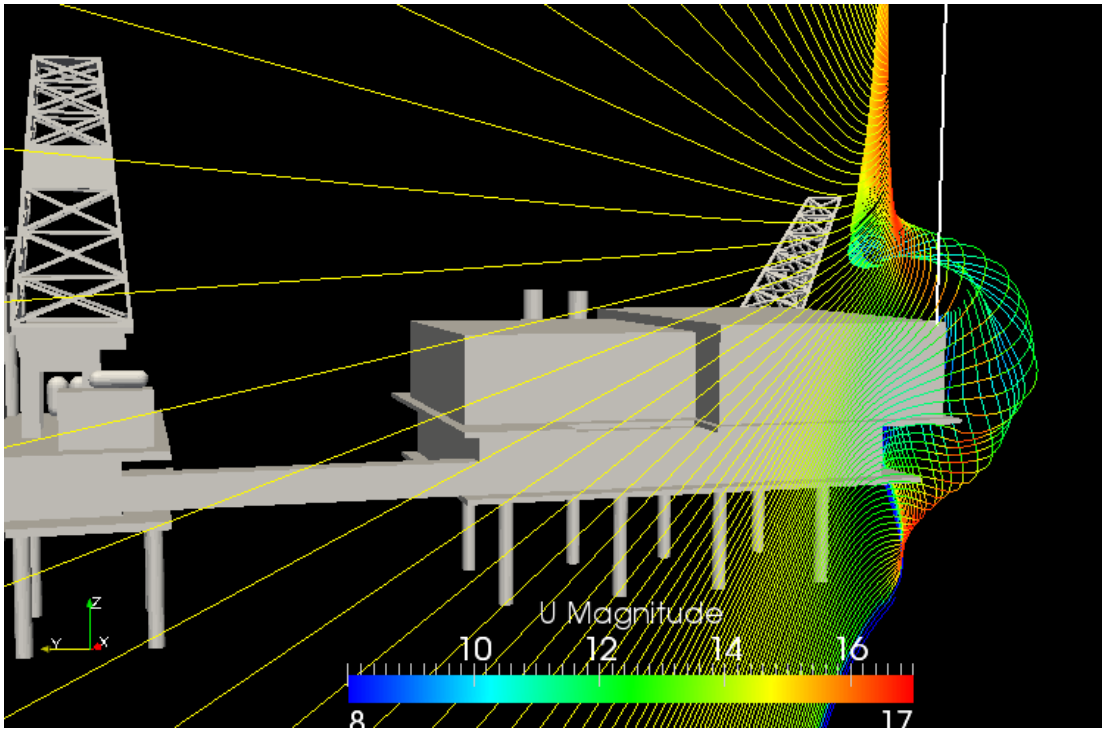

Figure 44: Velocity streamlines for Beatrice angle 300º

4.1.2 Velocity profile behind a complex geometry such as the derrick

One of the main characteristics of the Beatrice platform is a derrick which is situated in the middle of the drilling platform. The model for the CFD simulation was created using the CAD software and great attention was focused on the derrick geometry. In order to assess how well the OpenFOAM simulation could capture a complex flow distortion, velocity measurements in the wind tunnel were taken just behind the derrick with the flow going through the derrick first. The velocity measurements were compared with the CFD data. The experiment in the wind tunnel was carried out with the model in position angle 0°and in position angle 270°. Figures 45 and 46 show the velocity streamlines from the OpenFOAM simulation with the model in the

2 different positions. The white vertical line represents the position on which velocity measurements were taken in the wind tunnel. Measurements were taken every 1 cm from the bottom of the line corresponding to the bottom level of the derrick up to 50 cm (the height of the derrick being 25 cm).

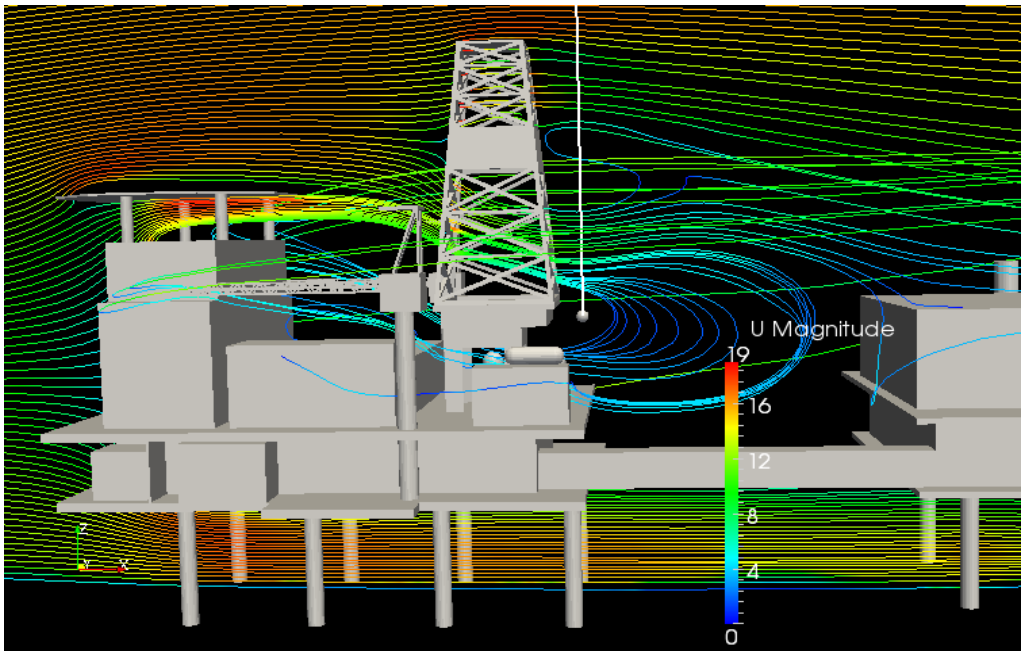

Figure 45: Velocity streamline for Beatrice angle 0º

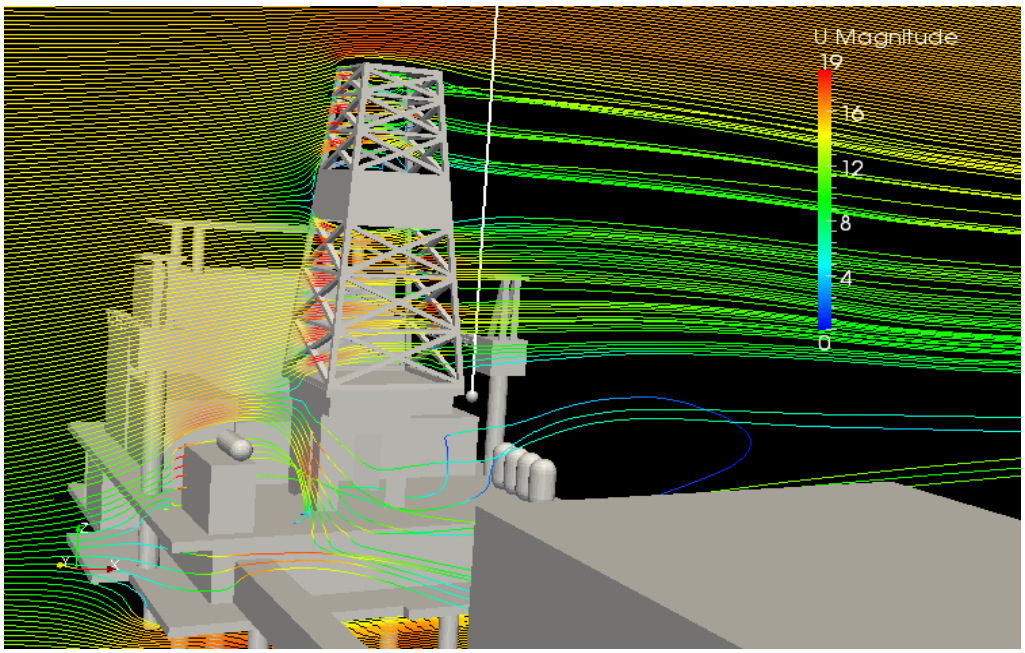

Figure 46: Velocity streamline for Beatrice angle 270º

Figure 47 reports the experimental velocity profile and the CFD data for these two positions. The experimental data and the CFD data were in very reasonable agreement and the flow distortion behind the derrick appears to have been well captured by the CFD study in both cases.

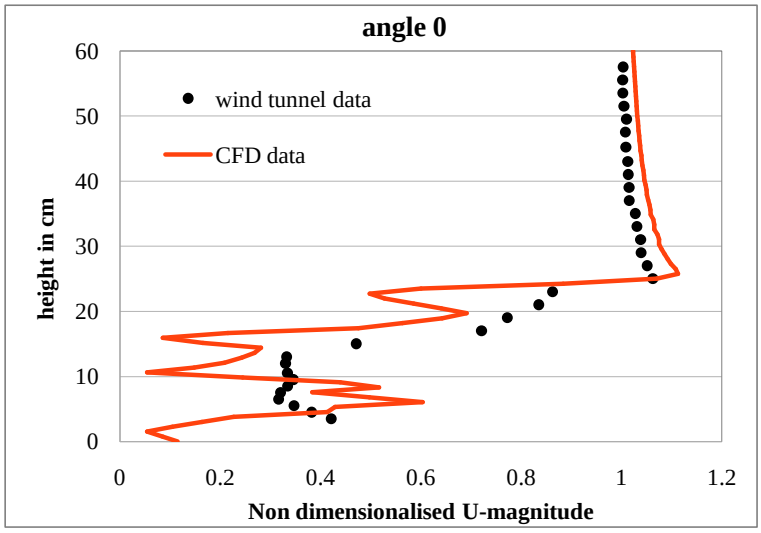

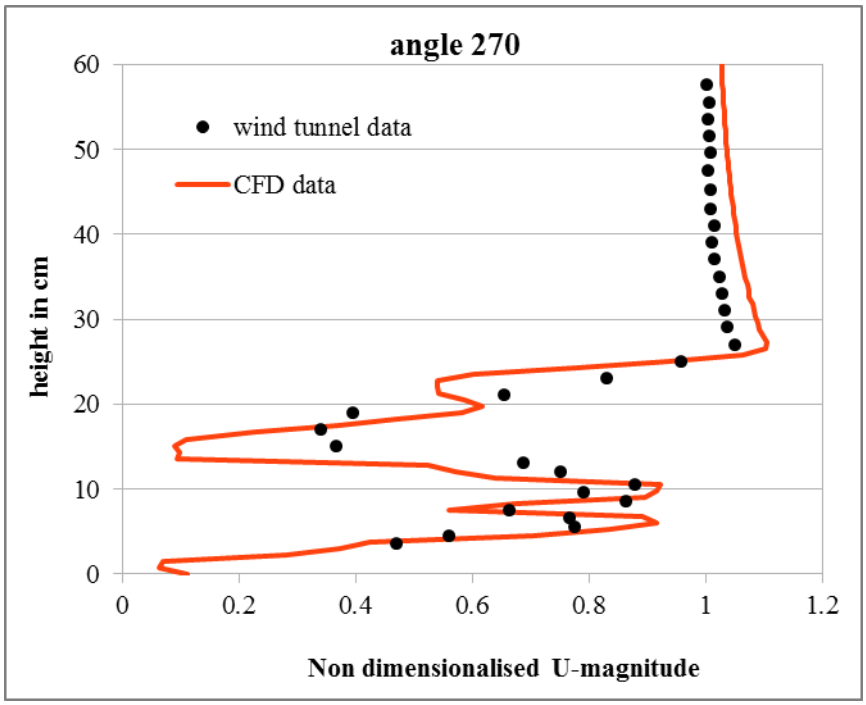

Figure 47: Velocity profile behind the derrick for positions angle 0° angle 270°

4.2 Results for Berlengas Island

4.2.1 Mesh sensitivity

Mesh sensitivity studies were carried out in order to assess the influence of mesh size on the predicted flow field. The result (Figure 48) shows that there was little change between the smallest grid (0.7 milion cells) and the largest (2 million cells) and a mesh size of 1 to 2 million cells was employed for each flow angle.

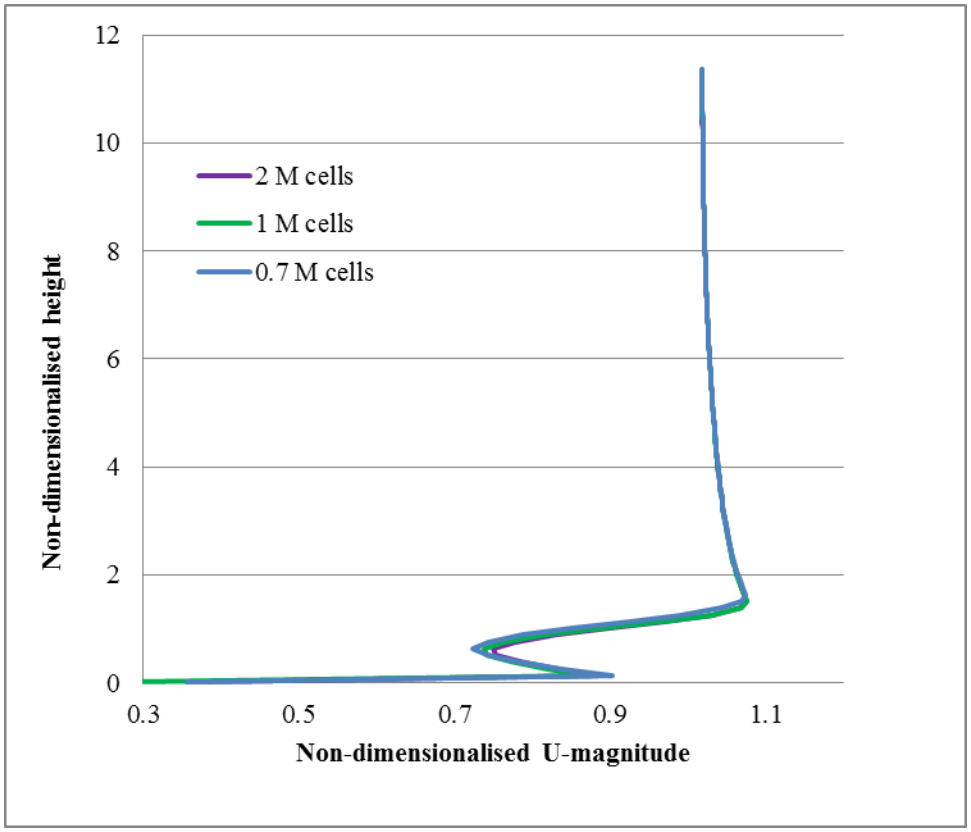

Figure 48: Mesh sensitivity analysis for the 210º flow angle case. Results show the velocity profile with height at lidar location.

4.2.2 Velocity profile: comparison of OpenFOAM data with wind tunnel data

Figure 49 shows the OpenFOAM-predicted velocity profile compared with the wind tunnel results for the 12 flow angles considered in the study.

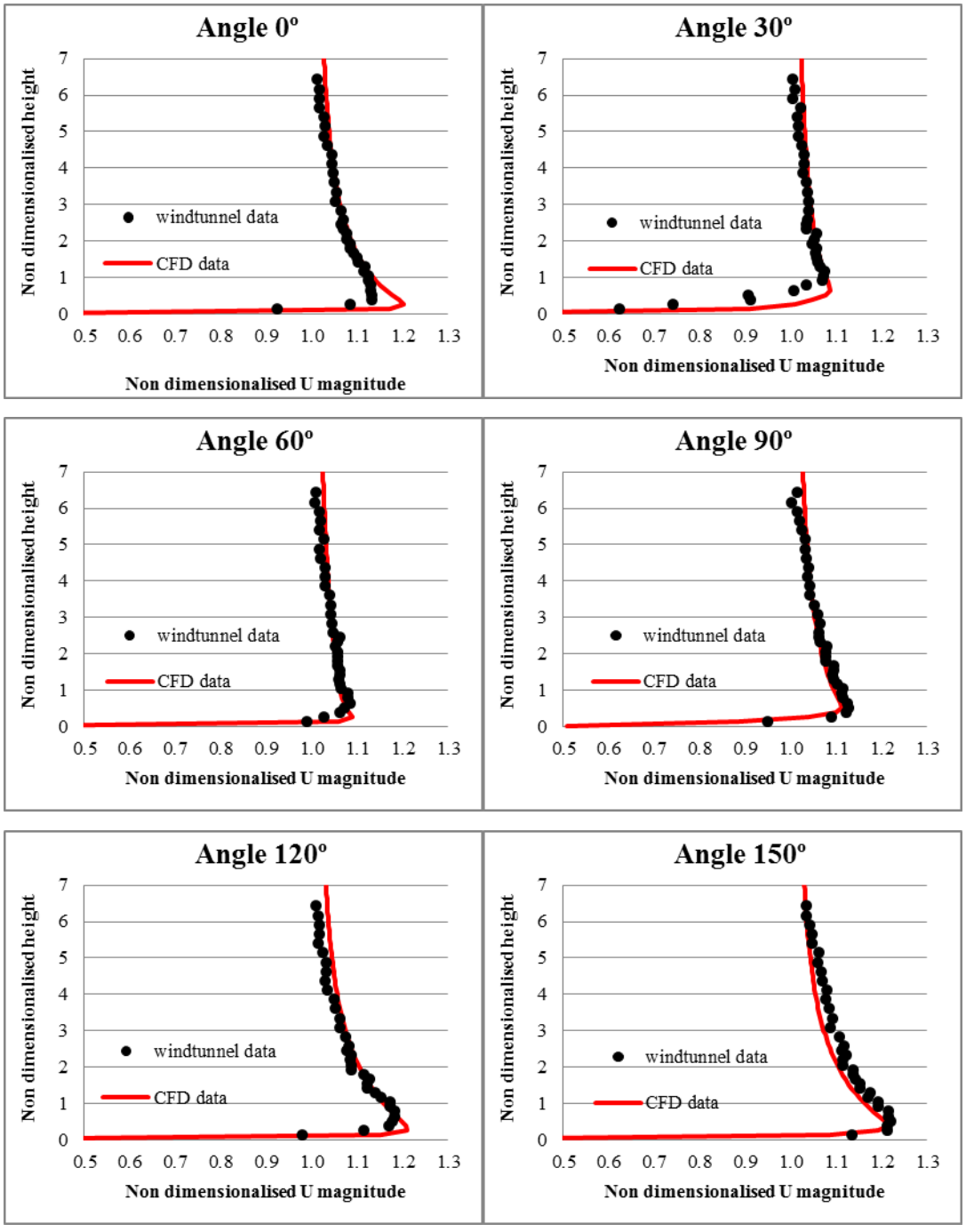

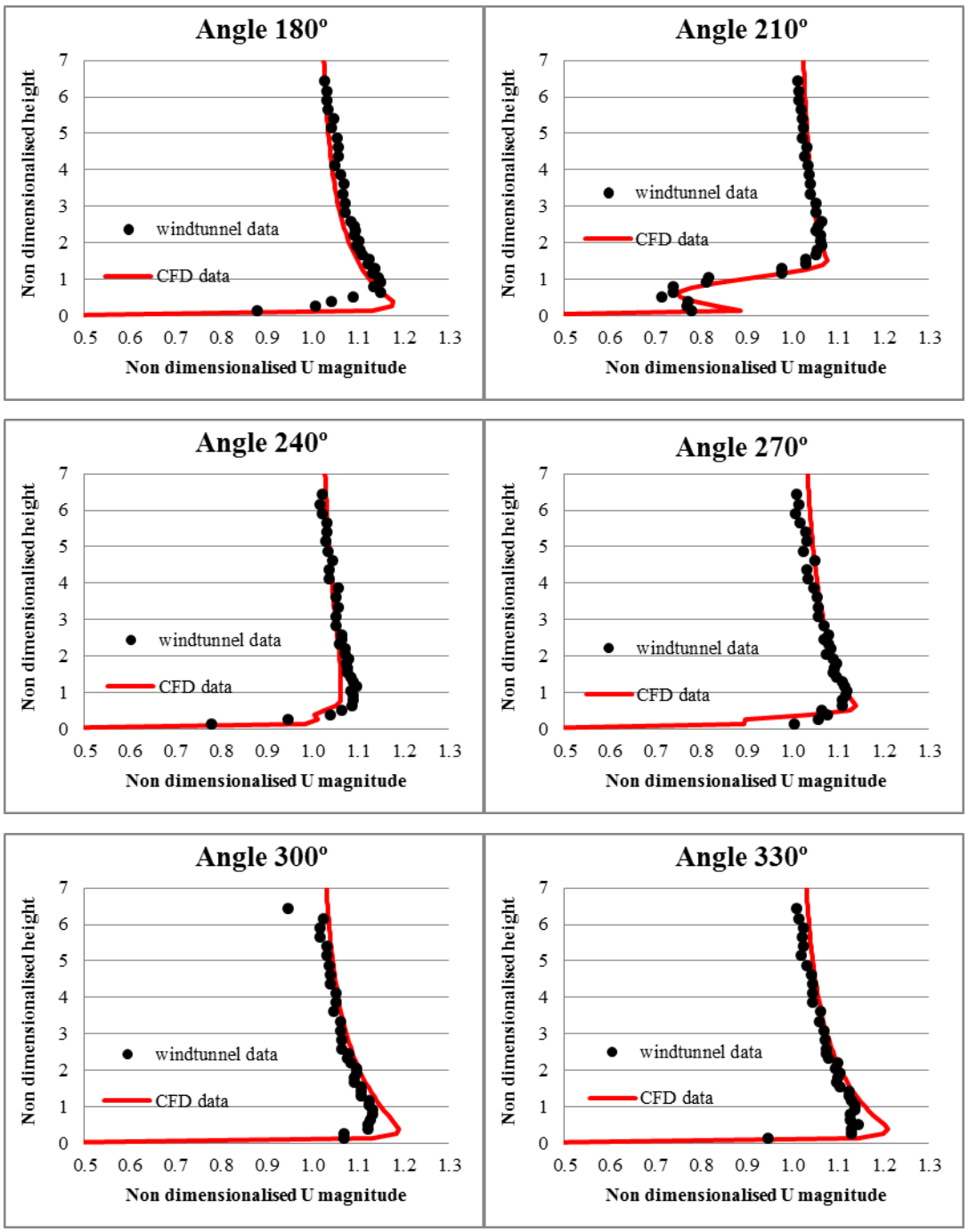

Figure 49: Comparison of velocity profile data openFoam/ wind tunnel

In general, the results showed a very good level of concurrence between the experimental wind tunnel measurements and the OpenFOAM CFD results.

Each flow angle represented a different challenge to the CFD study as the topology of the island coastline upstream of the measurement point varied greatly, including steep cliffs, rocky outcrops and escarpments. However, the general flow features of

flow acceleration and retardation above the island appear to have been captured very well by the CFD study. However, the velocity profile in the region close to the island for the flow angles 0º, 300º and 330º was not satisfactorily captured. Limitations in the ability of RANS turbulence models to pick-up regions of flow separation on relatively smooth surface offer a possible reason for this discrepancy. However, the general flow profile in the region likely to be assessed by any measuring equipment appears to have been adequately captured. Figure 50 shows typical complex flow features being captured around the island.

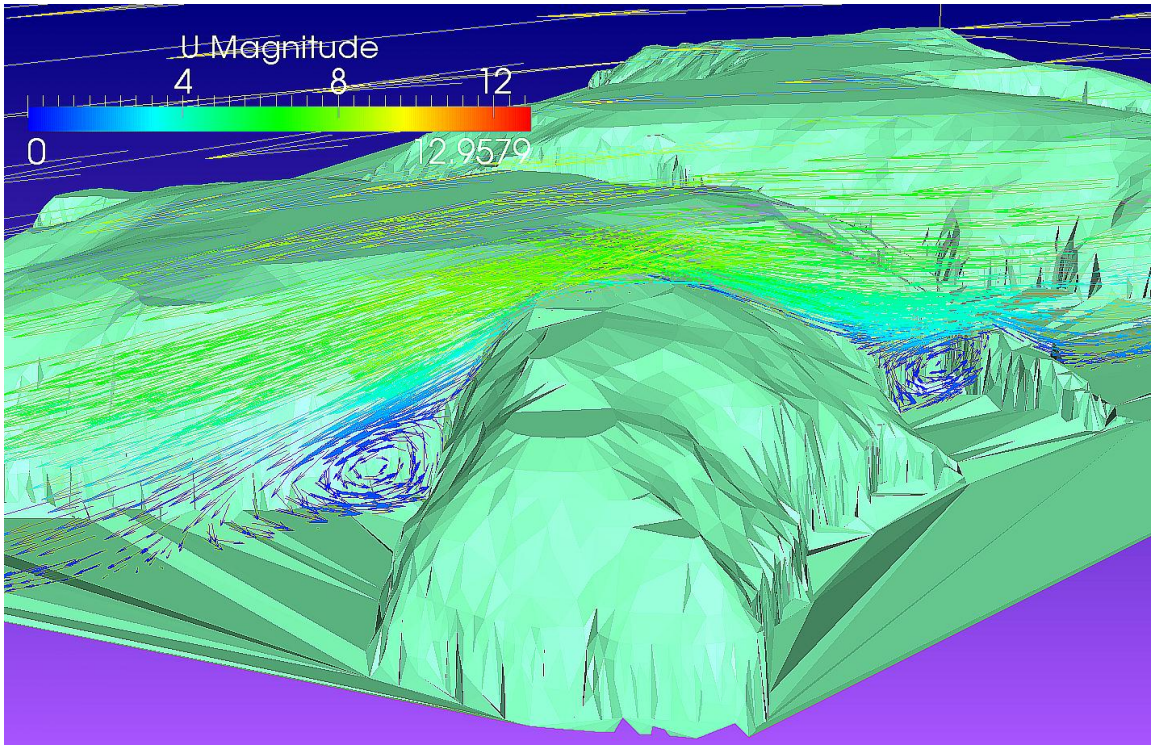

Figure 50: Velocity vectors showing flow separation and recirculation in the island canyons

4.3 Results for Fino3 mast

4.3.1 Velocity profile: comparison of OpenFOAM data with wind tunnel data

The openFOAM predicted velocity profile around the mast is reported in figure 51 below and compared with the wind tunnel data.

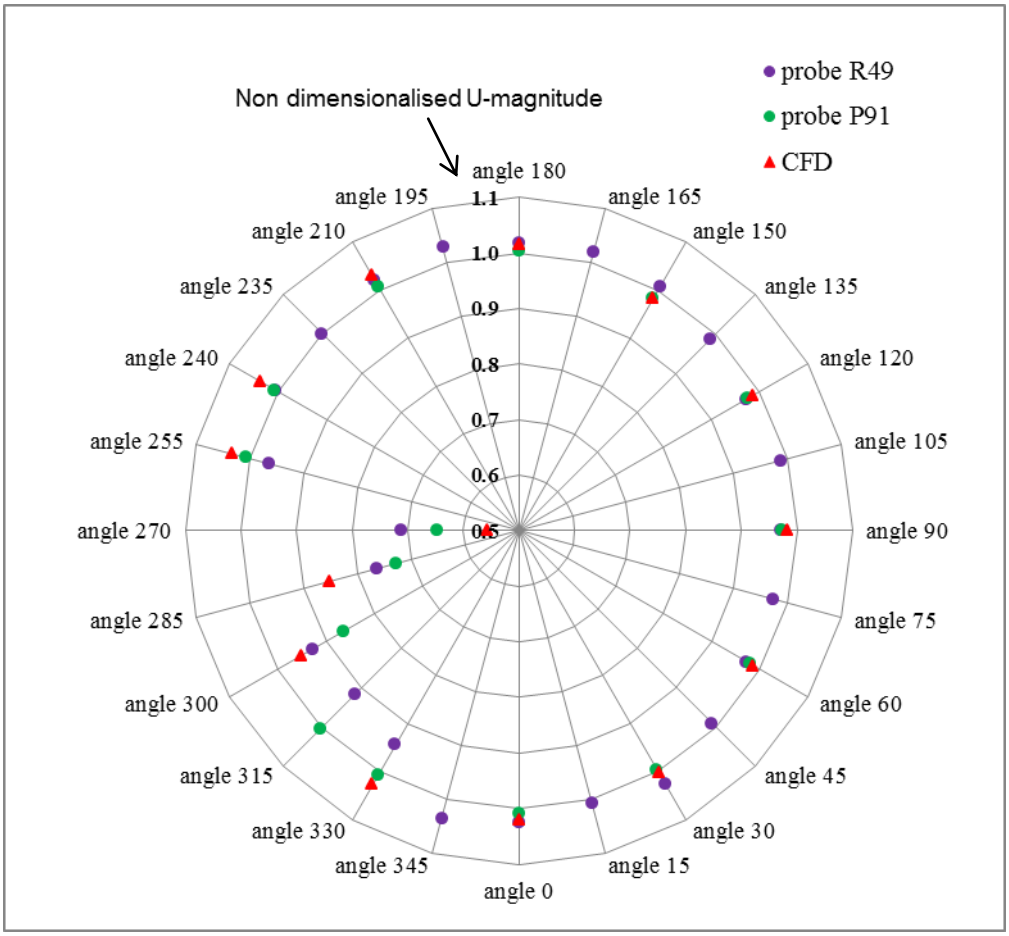

Figure 51: Comparison of velocity profile data OpenFOAM/ wind tunnel for FINO3 mast case

Comparison of OpenFOAM and wind tunnel data showed good agreement for wind speed measurements around the mast. The important flow distortion effect, when the model was between the angles 255° and 300°, was well picked up by the CFD simulation. The OpenFOAM predicted velocity profile along the boom with the

model in position angle 90° and angle 0° was also close to the experimental velocity profile as shown in figure 52.

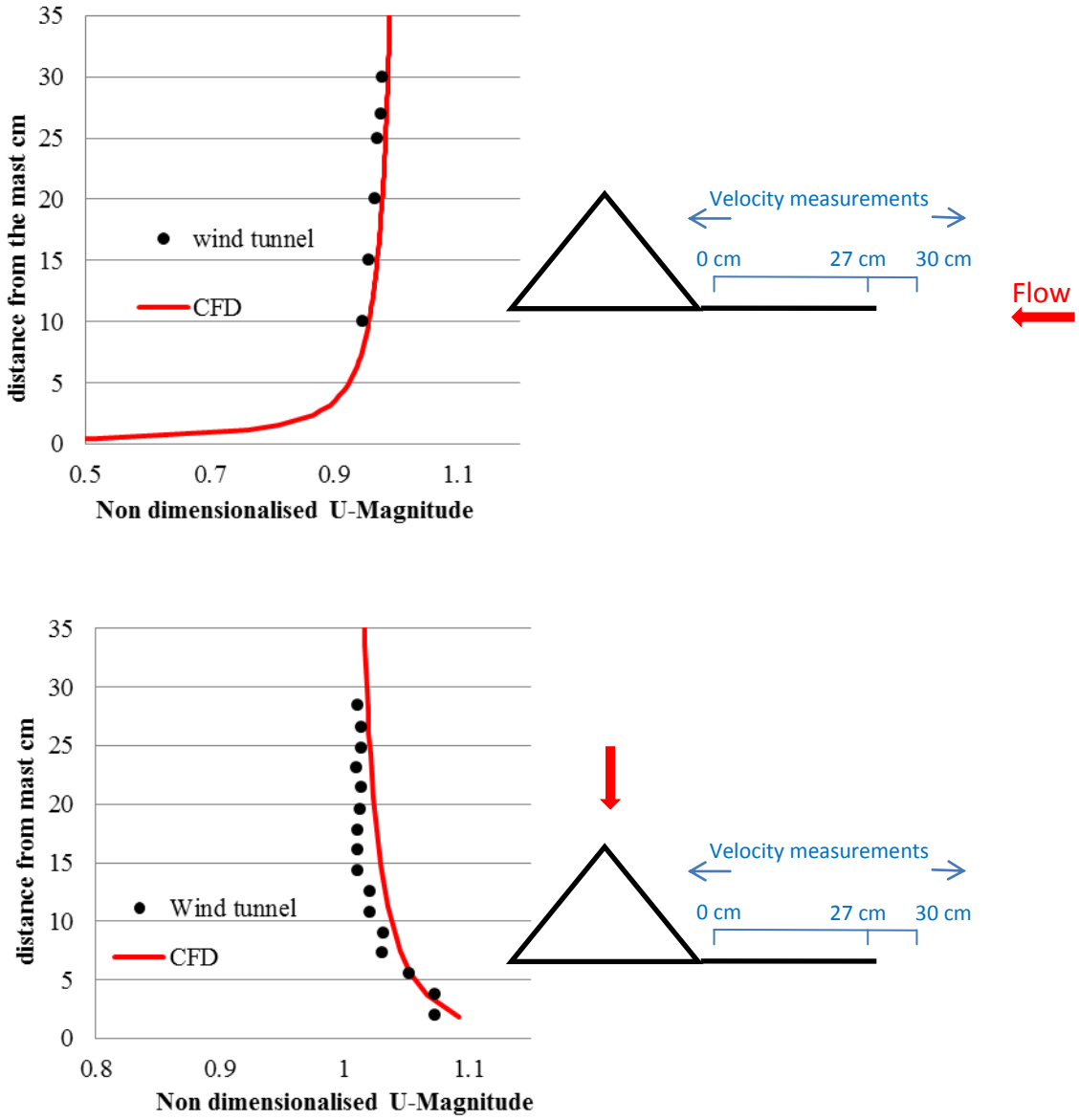

Figure 52: Velocity profile along the boom: experimental and CFD data

It is evident that the OpenFOAM solution has captured very well the flow features in the vicinity of the boom for these two different angles.

4.3.2 Scale up –up effect on the simulation

From summer 2009, the FINO3 mast has been recording wind speed data for the offshore wind industry. To date the effects of flow distortion on the measurements made by the instrumentation mounted on the three booms has not yet been quantitatively assessed. The CFD modelling of the flow field around the mast can provide an estimate of the amount of distortion that might be expected on the measuring equipment. In order to use the data of any simulation, it was important to check that the simulation solutions were Reynolds number independent. Therefore, a CFD simulation of a full scale model in position angle 0° was carried out and the velocity profile datafor full scale and model scale were compared. The velocity inlet for these both simulations was set up to 15 m/s. As the average wind speed expected in the North Sea should be around 6 m/s, a CFD simulation with a full scale model and an inlet velocity of 6m/s was also run. Velocity profiles above the end of the boom are reported in Figure 53.

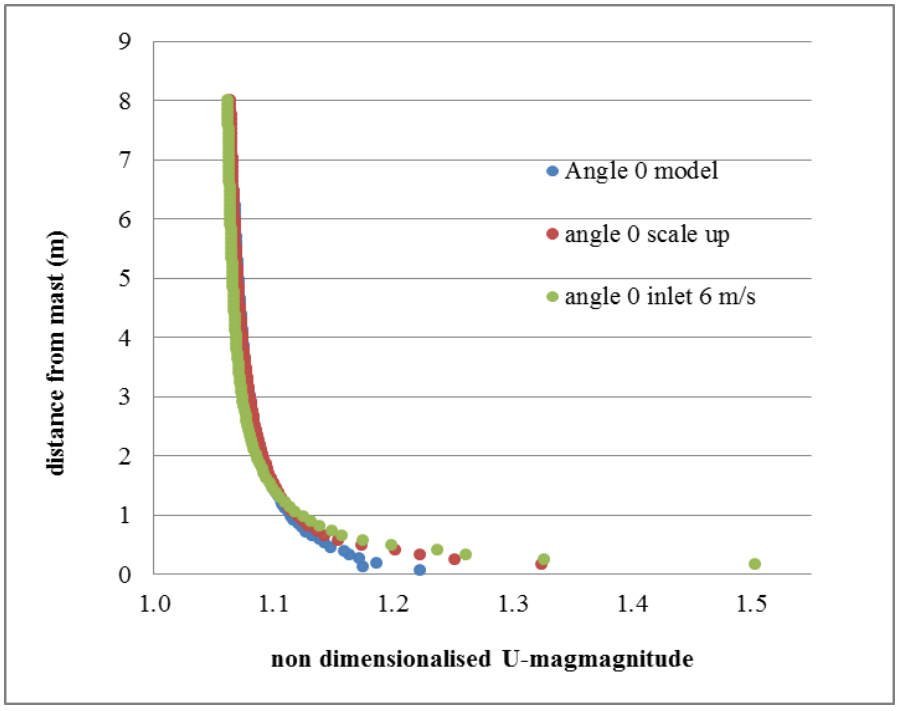

Figure 53: Velocity profile above boom for position angle 0° : data from the CFD modellisation of the sub-scale model, the full scale model, and the full scale model with inlet velocity at 6m/s

The graph shows a similar velocity profile for the 3 cases. This result confirmed the CFD solutions were indeed Reynolds number independent. Therefore, the CFD simulation could be used to obtain a better understanding of the interference effect due to the structure of the mast on anemometers mounted on the three different booms.

4.3.3 Distortion effect on the instrumentations

The CFD solutions were used to assess the distortion effect on the anemometers. Figure 54 represents the velocity contours around the mast for the 12 different positions. The wind direction for each case followed the x-direction represented as a red coordinate axis arrow on each graph. The positions of the three booms are shown as white lines. From the CFD solutions, the non dimensionalised velocity at the end of the three booms were extracted at the location where the anemometers were mounted. This value also represents the correction factor to apply to any velocity data recorded by the anemometers, and it is shown as a white number with the plots at the end of each boom.

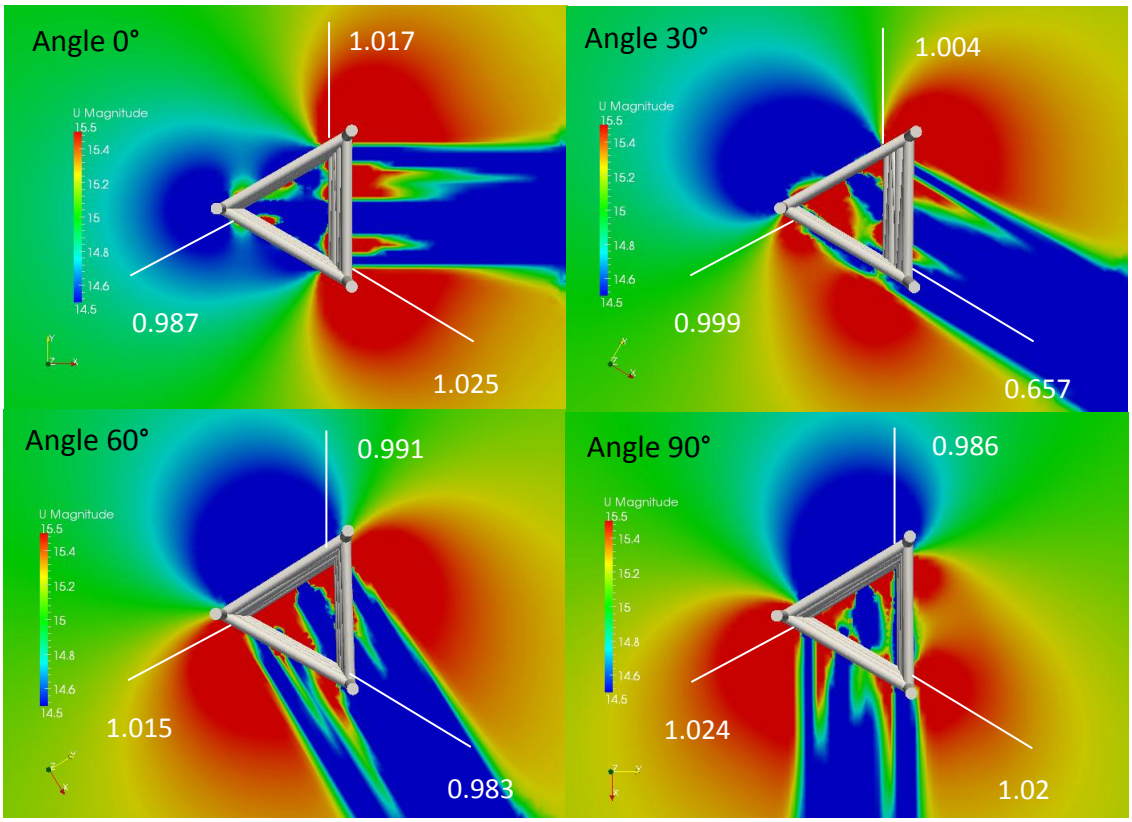

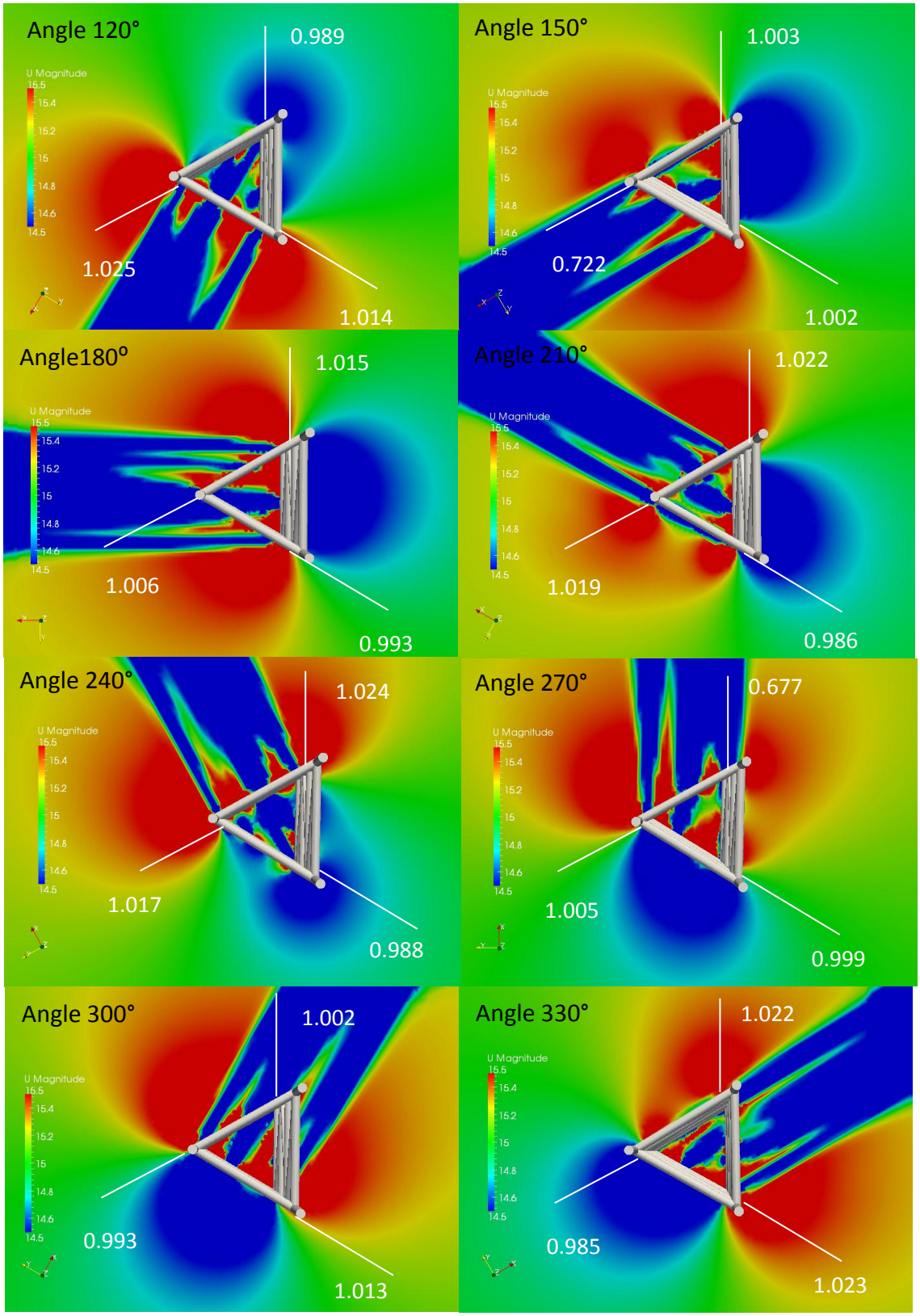

Figure 54: Velocity contours around the mast with correction factor for velocity data collected by the anemometers mounted on each boom

In general, any green area represents a velocity region not affected by the structure of the mast. The graphs show a deceleration of the velocity upstream and downstream (blue area) whereas acceleration of the velocity is reported as a red area. In the majority of cases, anemometers appear to be taking readings in or very close to an area where the flow field is affected by the mast. In order to check if a change in the length of the boom could prevent any anemometers to be in the distorted zone, velocity profiles along each boom were recorded. The Figure below describes the notation for the boom.

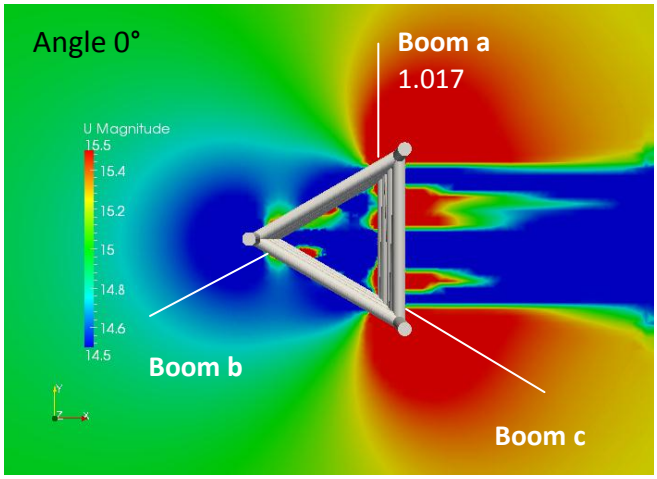

Figure 55: Velocity profile along each boom

Figure 56 displays the velocity profile just above each boom for the 12 different wind directions. In 3 cases (angle 30°, angle 150° and angle 270°), two of the booms were positioned in an area not affected by any distortion. In the other cases, the three booms appeared to be going through an area where the flow field was distorted and the data collected by the anemometers mounted at 5.4 m away from the mast should still be influenced by the distortion effect. Therefore, the wind velocity data should be filtered depending on the wind direction. Increasing the length of the boom from 5.4 m to 7 m would place any anemometer in an undisturbed flow field whatever the wind direction.

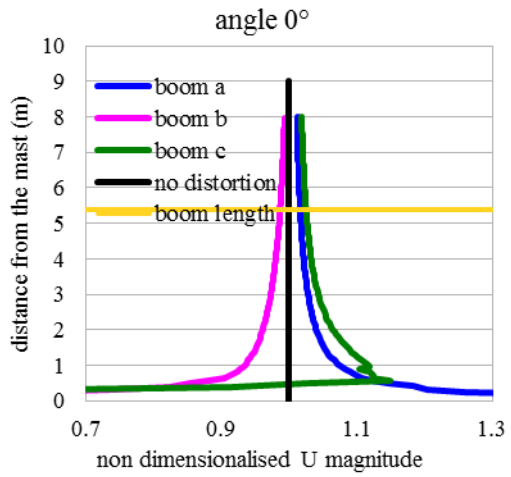
angle 0°
boom a
boom b
boom c
no distortion
boom length
distance from the mast (m)
non dimensionalised U magnitude

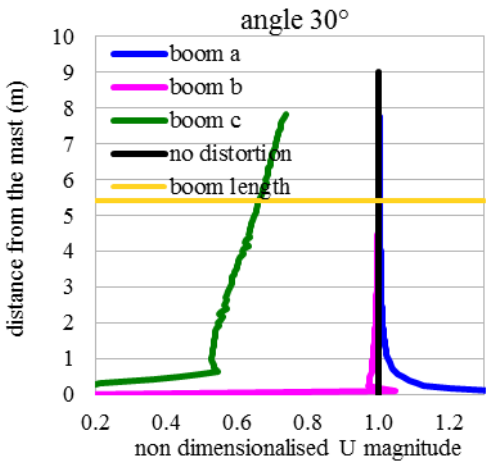
angle 30°
boom a
boom b
boom c
no distortion
boom length
distance from the mast (m)
non dimensionalised U magnitude

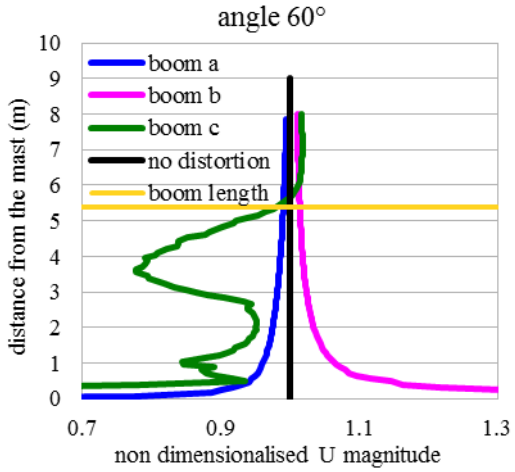
angle 60°
boom a
boom b
boom c
no distortion
boom length
distance from the mast (m)
non dimensionalised U magnitude

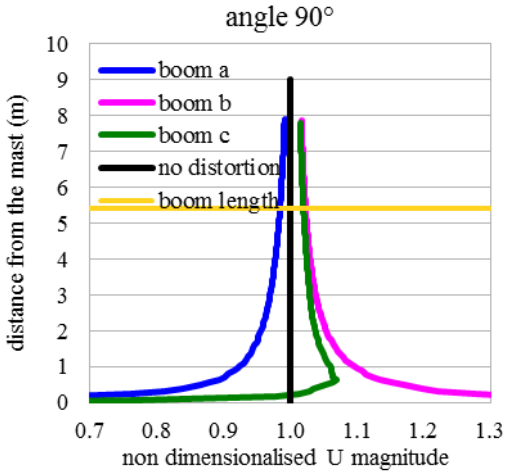
angle 90°
boom a
boom b
boom c
no distortion
boom length
distance from the mast (m)
non dimensionalised U magnitude

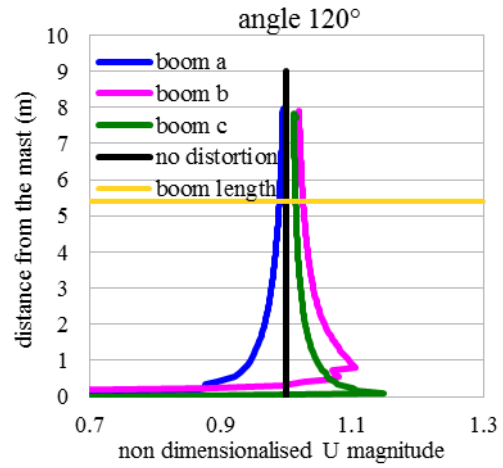
angle 120°
boom a
boom b
boom c
no distortion
boom length
distance from the mast (m)
non dimensionalised U magnitude

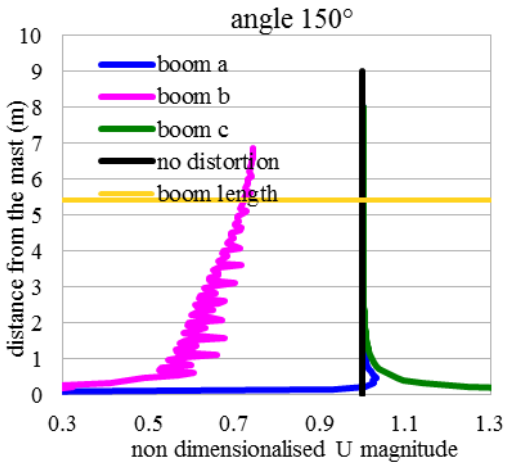
angle 150°
boom a
boom b
boom c
no distortion
boom length
distance from the mast (m)
non dimensionalised U magnitude

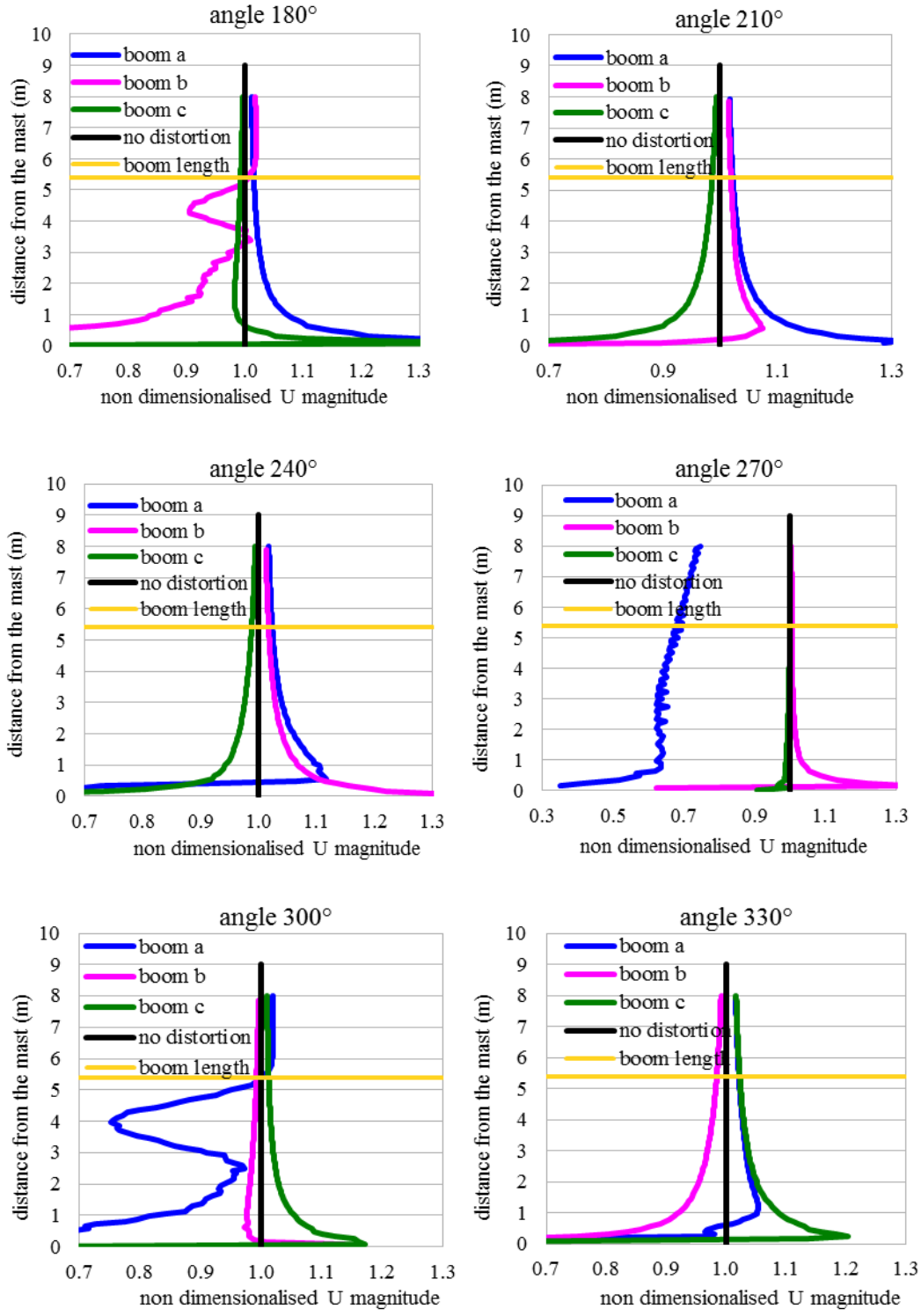

Figure 56: Velocity profile along each boom

5. CONCLUSION

OpenFOAM is a Computational fluid Dynamics package with an extensive range of features to solve complex fluid flow. It includes tools for meshing such as snappyHexMesh and for pre- and post- processing which can run in parallel. This allows the user to take full advantage of the computer hardware. But one of the main advantages of OpenFOAM is that its source code is publicly available and free. With a basic knowledge of C++ programming, it is easy to read, understand, modify and add further capability.

The performance and flexibility of OpenFOAM has been demonstrated for three specific examples. The CFD simulation of the air flow around three complex geometries was undertaken using a two equation turbulent model. The SnappyHexMesh meshing utilities worked well in all cases. Comparisons of OpenFOAM and wind tunnel studies showed, in general, very good agreement for wind speed measurements above or around the physical models. Flow distortion effects including acceleration or retardation velocity near the surface of the oil rig model was well picked up by the simulation. The velocity profiles behind a complex geometry such as a derrick from the CFD modelling was well matched to the experimental data. In the case of the Berlengas island, flow separation and recirculation features in island canyons was captured successfully. Finally, the flow distortion around a meteorology mast was also well quantified.

These results confirm that open source CFD solutions on a modest hardware budget are feasible for environmental flows over complex terrain or geometry. The cost benefits and open source nature of the OpenFOAM code mean that it has the potential reach a wider audience within the current wind energy analysis community.

6. REFERENCES

[1] EWEA: Wind in power, 2009 European statistics
February 2010

[2] EEA Technical report:
Europe's onshore and offshore wind energy potential
An assessment of environmental and economic constraints
No 6 / 2009

[3] Eurostat: Electricity production statistic
http://epp.eurostat.ec.europa.eu/statistics_explained/index.php/Electricity_production_and_market_trends

[4] OldBaum Services
http://www.oldbaumservices.co.uk/

[5] NORSEWInD
http://www.norsewind.eu/public/index.html

[6] M Courtney, R Wagner, P Lindelow, Testing and comparison of lidars for profile and turbulence measurements in wind energy.
In IOP Conference Series: Earth and Environmental Science 1, 2008

[7] Windcube http://leosphere.com/

[8] Landberg, L., Myllerup, L., Rathmann, O., Petersen, E. L., Jørgensen, B. H., Badger, J. and Mortensen, N. G., Wind resource estimation - an overview, *Wind Energy* 6 (3), pp. 261–271 (2003).

[9] Bowen, A. J. and Mortensen, N. G., Exploring the limits of WAsP: the wind atlas analysis and application program, *European Wind Energy Conference and Exhibition*, pp. 584–587. Gothenborg, Sweden (1996).

[10] Mortensen, N. G., Bowen, A. J. and Antoniou, I., Improving WAsP predictions in (too) complex terrain. *European Wind Energy Conference and Exhibition*, Athens, Greece (2006).

[11] Palma, J. M. L. M., Castro, F. A., Ribeiro, L. F., Rodrigues, A. H. and Pinto, A. P., Linear and nonlinear models in wind resource assessment and wind turbine micro-siting in complex terrain. *J. of Wind Engineering and Industrial Aerodynamics*, 96 (12), pp. 2308–2326, (2008).

[12] Perivolaris, Y. G., Vougiouka, A. N., Alafouzos, V. V., Mourikis, D. G., Zagorakis, V. P., Rados, K. G., Barkouta, D. S., Zervos, A. and Wang, Q., 2006 Coupling of a mesoscale atmospheric prediction system with a CFD microclimatic model for production forecasting of wind farms in complex terrain: Test case in the island of Evia. *European Wind Energy Conference and Exhibition*, Athens, Greece (2006).

[13] Wood, N., Wind flow over complex terrain: A historical perspective and the prospect for large-eddy modelling. *Boundary-Layer Meteorology*, 96 (1), pp. 11–32, (2000).

[14] Undheim, O., Andersson, H. and Berge, E., Non-linear, microscale modelling of the flow over Askervein Hill, *Boundary-Layer Meteorology*, 120 (3), 477–495, (2006).

[15] Hargreaves, D. M. and Wright, N. G., On the use of the k-ε model in commercial CFD software to model the neutral atmospheric boundary layer, *J. of Wind Engineering and Industrial Aerodynamics,* 95 (5), 355–369, (2007).

[16] Kanda, M., Progress in the scale modeling of urban climate: Review, *Theoretical and Applied Climatology*, 84 (1-3), 23-33, (2006).

[17] Ahmad, K., Khare, M. and Chaudry, K. K., Wind tunnel simulation studies on dispersion at urban street canyons and intersections - a review, *Journal of Wind Engineering and Industrial Aerodynamics*, 93 (9), 697-717, (2005).

[18] Tieleman, H. W., Wind tunnel simulation of wind loading on low-rise structures: a review, *Journal of Wind Engineering and Industrial Aerodynamics*, 91, 12-15, 1627-1649, (2003).

[19] Cermak, J. E. Wind-tunnel development and trends in applications to civil engineering, *Journal of Wind Engineering and Industrial Aerodynamics*, 91 (3), 355-370, (2003).

[20] Khanduri, A. C., Stathopoulos, T. and Bedard, C., Wind-induced interference effects on buildings - a review of the state-of-the-art, *Engineering Structures*, 20 (7), 617-630, (1998).

[21] Stathopoulos, T., Computational wind engineering: Past achievements and future challenges, *Journal of Wind Engineering and Industrial Aerodynamics*, 67 (8), 509-532, (1997).

[22] Kasperski, M. Design wind loads for low-rise buildings: A critical review of wind load specifications for industrial buildings, *Journal of Wind Engineering and Industrial Aerodynamics*, 61 (2-3), 169-179, (1996).

[23] H.K. Versteeg, W. Malalasekera: *An introduction to Computational Fluid Dynamics*, *The finite Volume Method*, second edition.

7. APPENDIX: stl geometry